2-1-2020

Synthesis, characterization, DNA binding, topoisomerase inhibition, and apoptosis induction studies of a novel cobalt(III) complex with a thiosemicarbazone ligand

Stephen J. Beebe
The Frank Reidy Center for Bioelectrics

Michael J. Celestine
Department of Chemistry and Biochemistry, Old Dominion University

Jimmie L. Bullock
Department of Chemistry and Biochemistry, Old Dominion University

Shayna Sandhaus
Department of Chemistry and Biochemistry, Biomolecular Sciences Institute, Florida International University, 11200 SW 8th St., Miami, FL 33199, USA., ssandhau@fiu.edu

Jessa Faye Arca
Department of Chemistry and Biochemistry, The University of Southern Mississippi

See next page for additional authors

Recommended Citation

Beebe SJ, Celestine MJ, Bullock JL, Sandhaus S, Arca JF, Cropek DM, Ludvig TA, Foster SR, Clark JS, Beckford FA, Tano CM, Tonsel-White EA, Gurung RK, Stankavich CE, Tse-Dinh YC, Jarrett WL, Holder AA. Synthesis, characterization, DNA binding, topoisomerase inhibition, and apoptosis induction studies of a novel cobalt(III) complex with a thiosemicarbazone ligand. J Inorg Biochem. 2020 Feb;203:110907. doi: 10.1016/j.jinorgbio.2019.110907. Epub 2019 Nov 2. PMID: 31715377; PMCID: PMC7053658.

Published in final edited form as:

J Inorg Biochem. 2020 February ; 203: 110907. doi:10.1016/j.jinorgbio.2019.110907.

Synthesis, characterization, DNA binding, topoisomerase inhibition, and apoptosis induction studies of a novel cobalt(III) complex with a thiosemicarbazone ligand

Stephen J. Beebe[a], **Michael J. Celestine**[b], **Jimmie L. Bullock**[b], **Shayna Sandhaus**[c], **Jessa Faye Arca**[d], **Donald M. Cropek**[e], **Tekettay A. Ludvig**[b], **Sydney R. Foster**[b], **Jasmine S. Clark**[b], **Floyd A. Beckford**[f], **Criszcele M. Tano**[b], **Elizabeth A. Tonsel-White**[b], **Raj K. Gurung**[b], **Courtney E. Stankavich**[b], **Yuk-Ching Tse-Dinh**[c], **William L Jarrett**[g], **Alvin A. Holder**[b,*]

[a]The Frank Reidy Center for Bioelectrics, 4211 Monarch Way, Suite 300, Norfolk, VA 23529, USA

[b]Department of Chemistry and Biochemistry, Old Dominion University, 4541 Hampton Boulevard, Norfolk, VA 23529, USA

[c]Department of Chemistry and Biochemistry, Biomolecular Sciences Institute, Florida International University, 11200 SW 8th St., Miami, FL 33199, USA

[d]Department of Chemistry and Biochemistry, The University of Southern Mississippi, 118 College Drive, Hattiesburg, MS 39406, USA

[e]U.S. Army Corps of Engineers, Construction Engineering Research Laboratory, Champaign, IL 61822, USA

[f]The University of Virginia's College at Wise, 1 College Avenue, Wise, VA 24293, USA

[g]School of Polymers and High-Performance Materials, The University of Southern Mississippi, 118 College Drive, #5050, Hattiesburg, MS 39406, USA

Abstract

In this study, 9-anthraldehyde-N(4)-methylthiosemicarbazone (MeATSC) **1** and $[Co(phen)_2(O_2CO)]Cl{\cdot}6H_2O$ **2** (where phen = 1,10-phenanthroline) were synthesized. $[Co(phen)_2(O_2CO)]Cl{\cdot}6H_2O$ **2** was used to produce anhydrous $[Co(phen)_2(H_2O)_2](NO_3)_3$ **3**. Subsequently, anhydrous $[Co(phen)_2(H_2O)_2](NO_3)_3$ **3** was reacted with MeATSC **1** to produce $[Co(phen)_2(MeATSC)](NO_3)_3{\cdot}1.5H_2O{\cdot}C_2H_5OH$ **4**. The ligand, MeATSC **1** and all complexes were characterized by elemental analysis, FT IR, UV–visible, and multinuclear NMR (^1H, ^{13}C, and ^{59}Co) spectroscopy, along with HRMS, and conductivity measurements, where appropriate. Interactions of MeATSC **1** and complex **4** with calf thymus DNA (ctDNA) were investigated by carrying out UV–visible spectrophotometric studies. UV–visible spectrophotometric studies revealed weak interactions between ctDNA and the analytes, MeATSC **1** and complex **4** (K_b = 8.1

*Corresponding author. aholder@odu.edu (A.A. Holder).

Declaration of competing interest

There is no interest conflict in this paper.

Appendix A. Supplementary data

Supplementary data to this article can be found online at https://doi.org/10.1016/j.jinorgbio.2019.110907.

× 10^5 and 1.6 × 10^4 M^{-1}, respectively). Topoisomerase inhibition assays and cleavage studies proved that complex **4** was an efficient catalytic inhibitor of human topoisomerases I and IIα. Based upon the results obtained from the 3-(4,5-dimethylthiazol-2-yl)-5-(3-carboxymethoxyphenyl)-2-(4-sulfophenyl)-2H-tetrazolium (MTS) assay on 4T1-luc metastatic mammary breast cancer cells (IC_{50} = 34.4 ± 5.2 μM when compared to IC_{50} = 13.75 ± 1.08 μM for the control, cisplatin), further investigations into the molecular events initiated by exposure to complex **4** were investigated. Studies have shown that complex **4** activated both the apoptotic and autophagic signaling pathways in addition to causing dissipation of the mitochondrial membrane potential ($\Delta\Psi_m$). Furthermore, activation of cysteine-aspartic proteases3 (caspase 3) in a time- and concentration-dependent manner coupled with the $\Delta\Psi_m$, studies implicated the intrinsic apoptotic pathway as the major regulator of cell death mechanism.

Keywords

Cobalt(III) complex; Thiosemicarbazone; Mitochondrial membrane potential; Calf thymus DNA; Breast cancer; ^{59}Co NMR spectroscopy

1. Introduction

Breast cancer (BCa) is the second leading cause of morbidity and mortality in women [1–5]. Furthermore, triple-negative breast cancer (TNBC) presents considerable therapeutic challenges due to disease heterogeneity, absence of established therapeutic targets, aggressive metastatic potential with higher rate of distant recurrence, and poor prognosis [6–8]. In addition, TNBC is most common in younger patients (TNBC is more likely to occur before age 40 or 50, versus age 60 or older, which is more typical for other breast cancer types [9,10]), especially in African American women [11] often leading to significant disease progression and poor prognosis.

Metastatic breast cancer is the most common disease in western women with approximately 1.7 million new breast cancer diagnoses in 2014 [12,13]. In many patients, it is not the primary tumor but metastases at distant sites that are the main cause of death. While rates of metastasis and mortality have slightly decreased over the last two decades, the disease is still considered incurable even with advances in early detection and systemic adjuvant therapies [14]. Chemotherapy only increases the 15-year survival rate of women under 50 by 10%; in elderly women this increase is only 3% [15,16]. No technology currently exists for the accurate prediction of metastasis; consequently, patients are subject to the toxic side effects of classic chemotherapy, which substantially affect the patients' quality of life [17–19]. Therefore, there is an urgent need to necessitate concerted efforts to identify effective agents against TNBC.

Cisplatin is widely used for the treatment of many cancers [20] despite its high toxicity, undesirable side effects, and problems with drug resistance in primary and metastatic cancers [21,22]. These limitations have spurred a growing interest in novel non-platinum metal complexes that show anti-cancer properties [23]. Several ruthenium- [24–26], gold-, gallium-, titanium-, vanadium, and arsenic-based compounds have been investigated for their anti-cancer potential [27–32]. Although none of these compounds have been approved

clinically, significant advancements have been made in their development including clinical studies with some of the most promising candidates. More recently, Jaouen and co-workers reported the use of ferrocenyl tamoxifen derivatives for breast cancer inhibition [33–35]. In one of those studies, Jaouen and co-workers [35] developed stealth FcOHTam, an organometallic ferrocene derivative of hydroxytamoxifen loaded lipid nanocapsules to evaluate this novel drug on a TNBC xenografted model [35]. A significantly lower tumor volume was obtained with a difference of 36% at day 38 when compared to the untreated group [35]. Those results represented the first evidence of an in vivo effect of FcOHTam and ferrocenyl derivatives on xenografted breast tumors [35].

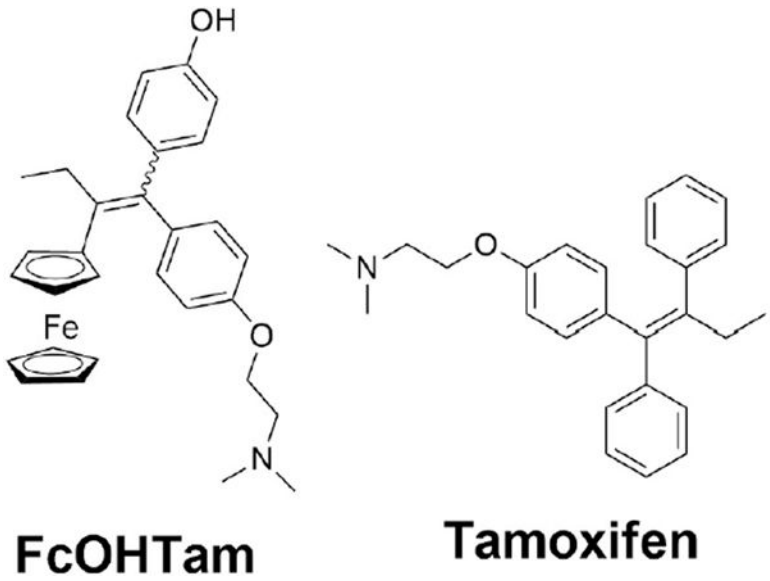

For many years, and more recently, the interaction between a variety of transition metals with polypyridyl ligands and DNA has been extensively studied as part of the efforts to fight cancer [36–45]. Due to unusual binding properties and general photoactivity, these coordination compounds are suitable candidates as DNA secondary structure probes, photocleaving agents, and anti-cancer drugs [46]. Examples of photocleaving activities with ruthenium(II)-containing mixed-metal complexes with rhodium(III) and vanadium(IV) metal centers were reported by Brewer and co-workers [42,43,47] and Holder and co-workers [48], and by other researchers who reported cobalt-, ruthenium-, and vanadium-containing metal centers [49–80].

Cobalt is one of the most important trace metals, where in the form of vitamin B_{12} (cobalamin), it plays a number of critical roles in multiple biological functions, including DNA synthesis, formation of red blood cells, maintenance of the nervous system, and growth and development. Despite their well-known versatility, cobalt-containing compounds have not been studied extensively as inorganic pharmaceuticals in comparison to other metals. To date, the only cobalt-based therapeutic that has reached clinical trials is Doxovir, a Co(III) Schiff base complex effective against drug-resistant herpes simplex virus 1 (HSV1) [81]. While it provides an example for cobalt-based pharmaceuticals, the mechanism of action of Doxovir is not fully understood. A substantial amount of literature on cobalt-

containing complexes has been reported while demonstrating their potential for medicinal applications [32,82–89]. However, the rationale behind the design and mechanisms of many of these agents has not been clearly defined.

Cobalt(III) and ruthenium(II) complexes that can intercalate between the stacked base pairs of native DNA have been actively investigated as probes [90–94] of DNA structure in solution and as stereoselective or conformation-specific agents for the photoactivated cleavage of DNA [95,96]. The nature of the interactions between cobalt (III) and ruthenium(II) complexes and others [97,98] and DNA have primarily been studied by cyclic voltammetry [96,99–104], spectroscopic [105–109], and X-ray crystallographic methods [105], to name a few.

Metal-based compounds that contain thiosemicarbazones as ligands possess a wide range of biological activities [110–117]. Thiosemicarbazones and their metal complexes present a wide range of applications that stretch from analytical chemistry, through pharmacology to nuclear medicine [118,119]. The biomedical activity of the thiosemicarbazones is enhanced by coordination to a transition metal ion [110–117,120,121]. Approximately 40% of drug candidates produced from combinatorial screening programs have poor aqueous solubility (< 10 μM) [122]. Coordination of a drug candidate to a positively-charged metal complex has been shown to greatly improve aqueous solubility in many cases, e.g., the proton pump inhibitor esomeprazole has very low aqueous solubility and is typically administered as esomeprazole magnesium, a water soluble bis(esomeprazole) magnesium complex [123]. Alternatively, coordination of a metal ion by negatively-charged groups such as carboxylates and phosphates can reduce the negative charge of a drug, thus enhancing passive cellular uptake and absorption [124]. In addition, endogenous metal ions and complexes can offer active transport pathways into the cell, allowing greater and more selective cellular accumulation of the drug [125].

Transition metal complexes are particularly suited to controlled drug release, having bonds that are highly responsive to their environment [121]. Such cases are applied when prodrug complexes can be designed that are inert under normal physiological conditions, but become labile with a change in environment such as redox status, pH, or the localized application of light [126–128]. By not activating a drug before it reaches its target, side reactions and premature metabolism that can lead to undesirable side effects to normal cells can be reduced tremendously [110–116,127,129]. In addition to overcoming the limitations of an organic drug, the metal complex can itself be biologically active [129]. By generating an active metal complex and active organic molecule from a single prodrug, multiple means of acting upon a target can be achieved [130]. Dual-action drugs may be more potent than the parent organic drug and be able to circumvent drug resistance mechanisms [131].

Cobalt(III) complexes with thiosemicarbazones and methyl-substituted 1,10-phenanthroline [132] as ligands, have been reported as anti-cancer agents in several cancer cell lines [87,133]. However, an understanding of how cobalt-containing complexes interact with biological systems to elicit chemotherapeutic effects is clearly necessary for the development of cobalt-based drugs [83].

Given the antineoplastic activities of thiosemicarbazone metal complexes [87,134–136], it is important to know their sites of action and mechanisms of cell death induction at the molecular level. A Nomenclature Committee on “Cell Death” has defined regulated cell death (RCD) mechanisms that include a number of different signaling scenarios beyond the initial introduction of programmed cell death or apoptosis as an alternative to necrosis [137]. The most common RCD mechanisms include apoptosis, programmed necrosis or necroptosis, and post-autophagic cell death [138,139]. For studies here, we have focused on apoptosis and autophagy. Apoptosis can be induced by extrinsic mechanisms through cell death receptors and/or intrinsic mechanisms that are initiated by heterogeneous intracellular signaling such as DNA damage and oxidative stress or hypoxia, among others. All of these intrinsic mechanisms involve mitochondria. Autophagy serves pro-survival functions as well as RCD signaling, depending on the stimulus, its intensity, and cellular context.

In our efforts to carry out anti-cancer studies with non-platinum-containing complexes, we have decided to focus on a cobalt(III) complex using our previously reported appended thiosemicarbazone with anthracene (9-anthraldehyde-N(4)-methylthiosemicarbazone (MeATSC) **1**) [140]. Anthracene derivatives are the most important class of ligands with high intrinsic fluorescence properties [141]. Anthracene derivatives have been investigated for their binding to DNA, and some are promising chemotherapeutic agents [142,143]. Anthracene itself has been reported to be effective against psoriasis [144]; while other anthracene derivatives tested for their anti-cancer activity include mitoxantrone, ametantrone, and bisantrene [145–147]. Mitoxantrone, ametantrone, and bisantrene have been suggested to elicit their activity by binding to DNA through groove/electrostatic as well as intercalative binding modes [145–147]. The azonafides [148] are a series of anthracene-based DNA intercalators which inhibit tumor cell growth in vitro at low nanomolar concentrations and are not affected by the multidrug resistance phenomenon (MDR), which is a logical choice to explore the use of our cobalt(III) complex with an anthracene-containing thiosemicarbazone ligand, MeATSC **1** [140]. Herein this paper presents mechanistic investigations of the combined effect of thiosemicarbazone pharmacophore with anthracene (MeATCS **1**) and complex **4** on a highly aggressive metastatic breast cancer cell line, 4T1-luc [149–151]. Interactions of the novel complex **4** with ctDNA and human topoisomerase, cytotoxicity studies, studies of induction of apoptosis and autophagy signaling pathways, along with the effect on the mitochondrial membrane potential ($\Delta\Psi_m$) are also discussed.

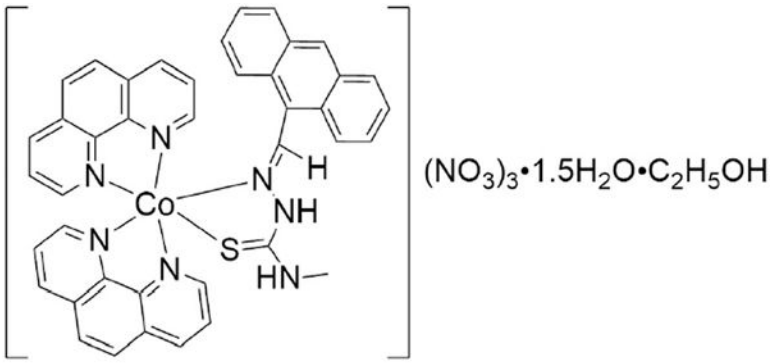

complex 4

2. Experimental

2.1. Reagents and instrumentation

All chemicals and reagents were purchased from commercial sources and were used without further purification. Ethidium bromide (EB) and calf thymus DNA (ctDNA) were purchased from Sigma-Aldrich (St. Louis, MO). Fetal bovine serum (FBS) and Dulbecco's Modified Eagle's Medium (DMEM) were obtained from Mediatech, Inc. (Manassas, VA). CellTiter 96® AQ_{ueous} One Solution Cell Proliferation Assay (MTS), and Caspase-3/7 Glo kits were purchased from Promega Corporation (Madison, WI). All buffer solutions were prepared with doubly-distilled water.

Microanalyses (C, H, and N) were performed by Columbia Analytical Services 3860 S. Palo Verde Road Suite 303 Tucson, AZ 85714, U.S.A., Galbraith Laboratories, 2323 Sycamore Dr. Knoxville, TN 37921, U.S.A., Intertek Chemical and Pharmaceuticals, 291 Route 22 East, Salem Industrial Park, Bldg. #5, Whitehouse, NJ 08888, U.S.A., and the College of Sciences Major Instrument Cluster (COSMIC), Old Dominion University, 143 Oceanography & Physical Sciences Building Norfolk, VA 23529, U.S.A. ^{59}Co NMR spectra were acquired on a Varian 500 MHz NMR spectrometer and on a Bruker AVANCE III 400 MHz NMR spectrometer with DMSO−d_6 as solvent, where $K_3[Co(CN)_6]$ (δ = 289 ppm [152]) as an external reference at room temperature. ^{1}H, ^{13}C, ^{1}H-^{1}H COSY, and ^{1}H-^{13}C HSQC NMR spectra were acquired on a Bruker AVANCE III 400 MHz NMR spectrometer with DMSO−d_6 as solvent. All NMR spectra were processed with the Spectrus Processor 2012 software which is available from Advanced Chemistry Development (ACD, Inc., 8 King Street East, Suite 107, Toronto, Ontario M5C 1B5, Canada).

All UV–visible spectra were acquired on an Agilent 8453A diode array spectrophotometer; while all conductivity measurements were acquired on a SPER Scientific 860032 benchtop conductivity/TDS/salinity meter. The meter was calibrated using a 1413 μS cm^{-1} NaCl conductivity standard solution available from VWR (Ricca Chemical Company, catalog #: RC2236.52–16). The cell constant, K, for the meter was calculated using a 0.0200 M KCl solution. Conductivity measurements were acquired with a 1.0 mM complex **4** in CH_3CN and DMSO as solvents.

All ESI MS spectra were acquired via positive electrospray ionization on a Bruker 12 Tesla APEX–Qe FTICR-MS with and Apollo II ion source at the College of Sciences Major Instrument Cluster (COSMIC), Old Dominion University, 143 Oceanography & Physical Sciences Building Norfolk, VA 23529, U.S.A. Complexes **2**, $[Co(phen)_2(O_2CO)]$ PF_6, **3**, and $[Co(phen)_2(H_2O)_2](PF_6)_3$ were dissolved in methanol; while complex **4** was dissolved in acetonitrile:methanol (1:1) before being introduced by direct injection using a syringe pump with a flow rate of 2 μL s^{-1}. The data was processed using Bruker Daltonics Data Analysis Version 3.4.

2.2. Synthesis of the ligand and complexes

2.2.1. Synthesis of the ligand and $[Co(phen)_2(O_2CO)]PF_6$—

The ligand, 9-anthraldehyde-N(4)-methylthiosemicarbazone (MeATSC) **1**, was synthesized according to previously reported protocol [140]. $[Co(phen)_2(O_2CO)]Cl{\cdot}6H_2O$ (where phen = 1,10-phenanthroline) **2** was synthesized using the procedure as reported by Kashiwabara et al. [153]: Cobalt chloride hexahydrate (2.35 g, 10 mmol) in water (5 mL) and 30% H_2O_2 (2 mL) were mixed in an ice-bath; then the mixture was added drop wise to a slurry of $KHCO_3$ (6.0 g, 60 mmol) in water (6 mL) at 0 °C. After the addition, the reaction mixture was stirred at 0 °C for 30 min. 1,10-Phenanthroline (3.6 g, 20 mmol) was dissolved in aqueous ethanol (5 mL) and was added to the solution of $CoCl_2{\cdot}6H_2O$ and H_2O_2. The resulting solution was stirred for 1 h at 20 °C.

After stirring for 1 h, the temperature was raised to 33 °C and the stirring was continued for 2 h. The previously green solution turned red in color after stirring for 2 h. The temperature was again raised to 50 °C and water (5 mL) was added to the solution. The solution was stirred for one additional hour. Glacial acetic acid (1176 μL, 1.2 g, 20 mmol) in water (5 mL) was added drop wise to the solution over a period of 15 min. The stirring was continued at 50 °C for 2 h. After 2 h, glacial acetic acid (1176 μL) in water (5 mL) was again added drop wise to the solution over a period of 15 min. The reaction was stirred for additional 30 min at 50 °C. The reaction mixture was then filtered using gravity; then the filtrate was kept overnight whereby crystals were formed. The crystals were filtered off in a fine frit and the resulting mother liquor of the filtrate was concentrated to half volume; then cooled in the refrigerator overnight to form more crystals. The second set of red crystals were filtered from the mother liquor and air dried. All crystals were combined and weighed. Yield = 5.15 g (83%).

^{1}H NMR (400 MHz, DMSO−d_6) 9.28 (d, J = 7.92 Hz, 2 H), 9.22 (d, J = 4.84 Hz, 2 H), 8.93 (d, J = 7.70 Hz, 2 H), 8.50 (m, 4 H), 8.43 (m, 2 H), 7.84 (d, J = 4.62 Hz, 2 H), and 7.78 (m, 2 H).

^{1}H NMR (400 MHz, D_2O, δ/ppm) 9.35 (dd, J = 5.28, 1.10 Hz, 2 H), 9.11 (dd, J = 8.14, 1.10 Hz, 1 H), 8.67 (dd, J = 7.92, 1.32 Hz, 1 H), 8.45 (dd, J = 5.50, 3.08 Hz, 1 H), 8.27 (d, J = 8.80 Hz, 1 H), 8.16 (d, J = 9.02 Hz, 1 H), and 7.52–7.63 (m, 2 H).

^{13}C NMR (101 MHz, DMSO−d_6, δ/ppm) 163.14, 154.03, 151.58, 147.01, 146.78, 140.82, 139.77, 130.27, 130.13, 127.97, 127.76, 127.71, and 126.82.

Lit. [154] ^{1}H NMR (400 MHz, DMSO−d_6, δ/ppm) 9.24 (J = 5.36), 8.99 (J = 8.28), 8.55 (J = 7.62), 8.16 (J = 8.92), 8.04 (J = 8.89).

Lit. [154] ^{13}C NMR (101 MHz, DMSO−d_6, δ/ppm) 166.63, 154.45, 151.21, 147.43, 147.38, 141.37, 140.33, 130.92, 130.83, 128.12, 127.83, 128.66, and 126.47.

High resolution ESI MS (positive mode): For $[C_{25}H_{16}CoN_4O_3]^+$, found m/z = 479.0544 and calculated m/z = 479.0549 ($[M-Cl]^+$).

$[Co(phen)_2(O_2CO)]PF_6$ was synthesized by metathesis of the pure sample of $[Co(phen)_2(O_2CO)]Cl{\cdot}6H_2O$ **2** by using an aqueous solution containing NH_4PF_6. $[Co(phen)_2(O_2CO)]Cl{\cdot}6H_2O$ **2** (0.32 g, 0.51 mmol) was dissolved in hot water (50 mL) before NH_4PF_6 (3.0 g, 18 mmol) was added with stirring. The reaction mixture was allowed to cool to room temperature before it was filtered through a fine frit. The resulting residue was washed with water followed by diethyl ether before it was air dried. Yield: 0.29 g (91%).

High resolution ESI MS (positive mode): For $[C_{25}H_{16}CoN_4O_3]^+$, found m/z = 479.0546 and calculated m/z = 479.0549 ($[M-PF_6^-]^+$).

2.2.2. Synthesis of anhydrous $[Co(phen)_2(H_2O)_2](NO_3)_3$ 3 and $[Co(phen)_2(H_2O)_2](PF_6)_3$—Initially, $[Co(phen)_2(H_2O)_2](NO_3)_3{\cdot}2H_2O$ was synthesized by the acid hydrolysis of $[Co(phen)_2(O_2CO)]Cl{\cdot}6H_2O$ using a modified procedure as reported by Ye et al. [155]:

$[Co(phen)_2(O_2CO)]Cl{\cdot}6H_2O$ (3.02 g, 5.87 mmol) was mixed with 3 M HNO_3 (130 mL). The resulting mixture was heated until all solids were dissolved. The reaction mixture was then stirred at room temperature for 24 h. After which the mixture was concentrated on a steam bath before it was poured into a mixture of Et_2O:EtOH (112 mL, 1:1 v/v) and was placed in the freezer (−20 °C) overnight.

The mixture was then filtered; the residue was washed with ethanol, air dried and collected. The residue was once more dissolved in 3 M HNO_3 (20 mL); then the resulting mixture was poured into Et_2O:EtOH (1:1 v/v, 100 mL). The mixture was then placed into the freezer (−20 °C) overnight. The mixture was filtered, and the residue was air dried and collected before it was placed into a desiccator with concentrated H_2SO_4 for three days to produce anhydrous $[Co(phen)_2(H_2O)_2](NO_3)_3$ **3**, which was then used in the subsequent syntheses. Yield = 2.44 g (65%)

^{1}H NMR (400 MHz, D_2O, δ/ppm) 9.71 (d, J = 4.84 Hz, 2 H), 9.37 (d, J = 7.48 Hz, 2 H), 8.82 (d, J = 7.92 Hz, 2 H), 8.66 (s, 2 H), 8.54 (d, J = 9.02 Hz, 2 H), 8.36 (d, J = 8.80 Hz, 2 H), 7.61–7.69 (m, 2 H), and 7.48 (d, J = 5.50 Hz, 2 H).

Lit: [155] ^{1}H NMR (500 MHz, D_2O, δ/ppm): 9.59 (d, 1 H, J = 5.22 Hz), 9.24 (d, 1 H, J = 8.23 Hz), 8.69 (d, 1 H, J = 8.15 Hz), 8.52 (q, 1 H), 8.41 (d, 1 H, J = 8.72 Hz), 8.23 (d, 1 H, J = 8.90 Hz), 7.51 (q, 1 H) and 7.37 (d, 1 H, J = 5.5 Hz).

High resolution ESI MS (positive mode) in methanol: For $[C_{24}H_{16}CoN_4O_2]^+$, found m/z = 451.0599 and calculated m/z = 451.0600 ($[M-3NO_3^- - H_2 - 2H^+]^+$). For $[C_{24}H_{18}CoN_4O_2]^+$, found m/z = 453.0757 and calculated m/z = 453.0756 ($[M-3NO_3^- - 2H^+]^+$).

$[Co(phen)_2(H_2O)_2](PF_6)_3$ was synthesized by metathesis of the pure sample of anhydrous $[Co(phen)_2(H_2O)_2](NO_3)_3$ **3** with an aqueous solution containing NH_4PF_6: Anhydrous $[Co(phen)_2(H_2O)_2](NO_3)_3$ **3** (0.32 g, 0.50 mmol) was dissolved in hot water (10 mL) before NH_4PF_6 (3.00 g, 18 mmol) was added. The mixture was cooled to room temperature before it was filtered through a fine frit. The resulting residue was washed with water, followed by diethyl ether, then air dried. Yield = 0.29 g (65%).

High resolution ESI MS (positive mode) in methanol: For $[C_{24}H_{18}CoN_4O_2]^+$, found m/z = 453.0760 and calculated m/z = 453.0756 ($[M-3NO_3^- - 2H^+]^+$).

2.2.3. Synthesis of $[Co(phen)_2(MeATSC)](NO_3)_3 \cdot 1.5H_2O \cdot C_2H_5OH$ 4—Anhydrous $[Co(phen)_2(H_2O)_2](NO_3)_3$ **3** (0.79 g, 1.2 mmol), MeATSC (0.37 g, 1.3 mmol), and absolute ethanol (400 mL) were mixed in a 1 L round bottom flask. The reaction mixture was degassed with argon for 15 min, then refluxed with stirring for 24 h at 110 °C. The reaction mixture was then evaporated to dryness, and the resulting residue was sonicated with diethyl ether before it was filtered through a fine frit. The residue was washed thoroughly with diethyl ether until the filtrate was colorless; then air dried. Yield: 1.03 g (88%).

Anal. calculated for $C_{43}H_{40}CoN_{10}O_{11.5}S$ (MW = 971.84): calculated; C, 53.14; H, 4.15; and N, 14.41%.

Found: C, 53.23; H, 3.73; and N, 14.14%.

High resolution ESI MS (positive mode) in acetonitrile:methanol: For $[C_{41}H_{30}CoN_7S]^{2+}$, found m/z = 355.5798 and calculated m/z = 355.5802 ($[M-3NO_3^- - H^+]^{2+}$); and for $[C_{24}H_{16}CoN_4]^+$, found m/z = 419.0693 and calculated m/z = 419.0701 ($[M-3NO_3^- - MeATSC]^+$).

^{1}H NMR (400 MHz, DMSO−d_6, δ/ppm): 10.10 (d, J = 5.06 Hz, 1 H), 9.42 (d, J = 7.48 Hz, 1 H), 9.37 (d, J = 8.14 Hz, 1 H), 9.03 (d, J = 8.14 Hz, 1 H), 8.94 (d, J = 7.92 Hz, 2 H), 8.72 (dd, J = 8.03, 5.61 Hz, 1 H), 8.55–8.67 (m, 4 H), 8.47 (d, J = 8.80 Hz, 1 H), 8.51 (d, J = 8.80 Hz, 1 H), 8.26 (br. s., 1 H), 8.03–8.13 (m, 3 H), 7.98 (dd, J = 7.92, 5.50 Hz, 1 H), 7.69–7.84 (m, 3 H), 7.41–7.60 (m, 5 H) 3.30–3.49 (m), and 1.00–1.11 (m).

^{13}C NMR (101 MHz, DMSO−d_6, δ/ppm): 154.07, 153.47, 153.09, 152.79, 151.36, 146.78, 146.05, 145.66, 145.50, 145.26, 141.81, 141.49, 140.85, 140.26, 134.38, 131.83, 131.80, 131.18, 130.49, 130.08, 129.37, 129.00, 128.81, 128.62, 128.46, 128.30, 128.26, 128.22, 128.00, 127.69, 127.04, 126.74, 126.57, 125.55, 125.34, 124.74, 123.88, 64.72, 55.87, 31.28, 20.88, 18.39, and 14.99.

^{59}Co NMR (95 MHz, DMSO−d_6, δ/ppm): 7067 ppm.

UV–visible spectrum in DMSO (λ/nm ($\varepsilon/10^{-4}$ M^{-1} cm^{-1})): 264 (8.9), 355 (0.85), 372 (0.93), and 392 (1.0).

FTIR (ν/cm^{-1}): 3227 (s, br) and 3053 (s, br) (N–H), 1580 (m) (C═N), 1224 (s) and 827 (s) (C═S), and 1323 (vs) (NO_3^-).

Conductivity measurements (a 1.0 mM solution): In CH_3CN, Λ_m = 295 Ω^{-1} cm^{-1} mol^{-1} and in DMSO, Λ_m = 72 Ω^{-1} cm^{-1} mol^{-1}.

2.3. DNA-interaction studies

A stock solution of MeATSC **1** was prepared in DMSO, while the stock solution of complexes **3** and **4** were prepared in Tris-HCl buffer. All ctDNA stock solutions were prepared by dissolving commercially available ctDNA (0.11 g) in Tris-HCl buffer (100 mL, 5 mM Tris, 3.55 mM, 25 mM NaCl, pH 7.68); then stored at 4 °C for no longer than a week. UV absorbances at 260 and 280 nm of ctDNA in Tris-HCl buffer gave a ratio of 1.8–1.9, indicating that ctDNA was protein-free [156]. The ctDNA concentration in phosphate nucleotide was determined spectrophotometrically using a molar extinction coefficient of 6600 M^{-1} cm^{-1} at 260 nm [47].

The solutions of the analytes were prepared by diluting the respective species to a final concentration of 20 μM for MeATSC **1**, and 50 μM for complexes **3** and **4**, all in Tris-HCl buffer containing ctDNA at various concentrations ranging from 0 to 100 μM. The solutions were allowed to equilibrate for at least 5 min before their UV–visible spectra were acquired.

2.3.1. Stability studies of complex 4 in water and PBS buffer and its reactivity with reduced glutathione—

A 5 mM stock solution of complex **4** was prepared in DMSO before it was diluted to its final concentration of 20 μM in either water or PBS buffer (137 mM NaCl, 2.7 mM KCl, 10 mM Na_2HPO_4, and 2 mM KH_2PO_4, pH 7.20). Reduced *L*-glutathione stock was prepared in the PBS buffer and was diluted to a final concentration of 100 μM in the presence of 20 μM of complex **4**. The UV–visible spectra of the respective solutions were acquired at 0, 24, 48, 72, and 168 h.

2.4. Activity against topoisomerase I & II

2.4.1. Human topoisomerase I and IIα relaxation assay—

Human topoisomerase I (hTOP1, obtained from TopoGen in Buena Vista, CO) relaxation assays were carried out with 160 ng of supercoiled pBAD/Thio plasmid DNA purified by cesium chloride gradient centrifugation in the reaction buffer supplied by TopoGen. The DNA was mixed with the indicated concentration of compound dissolved in DMSO. Human topoisomerase I, 0.5 U, was then added to the mixture for a final volume of 20 μL. Following incubation at 37 °C for 30 min, the reactions were terminated by addition of 4 μL of a solution containing 5% sodium dodecyl sulfate (SDS), 0.25% bromophenol blue, and 25% glycerol. The samples were then analyzed by agarose gel electrophoresis [157]. The gels were stained in ethidium bromide and photographed under UV light before densitometry analysis.

Human topoisomerase IIα (hTOP2α, obtained from TopoGen) relaxation assays were carried out in the same manner as human topoisomerase I assays, but with 2 U of enzyme per reaction.

2.4.2. Human topoisomerase I and IIα cleavage assay—DNA cleavage assays were carried out with 300 ng of supercoiled pBAD/Thio plasmid DNA in 20 μL of buffer supplied by the manufacturer (TopoGen). DNA was first mixed with 0.5 μL of test compounds dissolved in DMSO. Five units of hTOP1 or 2.5 units of hTOP2α were then added, and the samples were incubated for 30 min at 37 °C before the addition of 2 μL stop solution (10% sodium dodecyl sulfate (SDS) and 20 mg mL^{-1} proteinase K). The samples were then incubated for an additional 30 min at 37 °C. The reactions were analyzed by electrophoresis in 1% agarose gels containing 0.5 μg mL^{-1} ethidium bromide before being photographed under UV light [158].

2.5. Cell culture

4T1-luc cells (mouse mammary breast cancer) were obtained from American Type Culture Collection (ATCC). 4T1-luc cells were transformed with pGL4.50*luc2*/CMV/H_{ygro}. 4T1-luc cells were maintained in the logarithmic stage of growth in high glucose Dulbecco's Modified Eagle's Medium (DMEM) supplemented with 10% fetal bovine serum (FBS), 1% non-essential amino acids (NEAA) and 1% antibiotics (100 units mL^{-1} penicillin and 100 μg mL^{-1} streptomycin) at 37 °C in a humidified atmosphere containing 5% CO_2 and were used at passages 3 to 25. Except where indicated, analyses were performed on same passage cells within two weeks after thawing. The cells used in these studies were tested and shown to be free of mycoplasma and viral contamination.

2.6. Cytotoxicity studies

Cell viability following exposure to complex **4** was assessed via the CellTiter 96® AQ_{ueous} One Solution Cell Proliferation (3-(4,5-dimethylthiazol-2-yl)-5-(3-carboxymethoxyphenyl)-2-(4-sulfophenyl)-2H-tetrazolium (MTS)) assay (Promega, Madison, WI). Briefly, the cells were seeded on a 96 well plate (2.5×10^4 cells per well) in 100 μL of medium and incubated for 4 h. Following incubation, solutions containing complex **4** were prepared in DMEM. The seeding media was removed, and cells were then treated with 100 μL complex **4** in complete media at different concentrations and incubated for 24 h at 37 °C in 5% CO_2. After 24 h of incubation, the cells were assayed for viability by the MTS assay as described by the manufacturer using μQuant™ Microplate spectrophotometer or VersaMax ELISA Microplate reader. To examine the effect of inhibition of the autophagic pathway, cells were pre-incubated at 37 °C for 4 h with 600 nM necrostatin-1 (Sigma-Aldrich, St. Louis, MO) prior to the addition of complex **4**. To examine the effect of inhibition of caspase activity, cells were pre-incubated with 10 mM benzyloxycarbonyl-Val-Ala-Asp-(*O*-methyl)-fluoromethylketone (z-VAD-FMK) for 4 h prior to the addition of complex **4**. Complex **4**, as well as all positive and negative controls, including cisplatin, were tested in triplicate on cells at various passage numbers.

2.7. Apoptosis evaluation

2.7.1. Caspase 3/7 activity—Caspase 3/7 activity was determined by Caspase-Glo 3/7 kit using tetrapeptide substrate sequences Ac-DEVD-AMC (Promega, Madison, WI). Following the manufacturer's instruction, for each analysis, the cells were plated in triplicate on 96-well plates (2.5×10^4 cells per well) in the presence or absence of pan caspase

inhibitor z-VAD-FMK for 4 h. The seeding media was removed, and the cells were then treated with 100 μL of complex **4** in complete media at different concentrations and incubated for 24 h at 37 °C in 5% CO_2. After a 24-hour incubation period, the plates were equilibrated at room temperature for 30 min before 100 μL of Caspase-Glo 3/7 reagent was added to each well. The contents were gently mixed using a plate shaker at 300 rpm for 30 s. The luminescence was read in a luminometer (FLUOstar Omega, BMG Labtech), after a 35-minute incubation at room temperature. The increase in activity was calculated based on activity of control (sham-treated) cells.

2.7.2. Measurement of mitochondrial membrane potential ($\Delta\Psi_m$)—The $\Delta\Psi_m$ was detected using tetramethylrhodamine ethyl ester (TMRE) (Immunochemistry Technologies LLC, Bloomington, MN) as previously described in the literature [159,160]. Briefly, cells were seeded on a 24 well plate (7.0×10^4 cells per well) for 4 h. After the incubation time, the medium was removed; then the cells were treated with 500 μL of complex **4**, all in complete media at different concentrations for either 2, 4, or 6 h at 37 °C in 5% CO_2. At the specified time points cells were then harvested using 150 μL trypsin-EDTA 1× (ThermoFisher Scientific, Waltham, MA), pelleted, and the supernatant was removed. The cells were then pre-incubated with 200 nM of TMRE for 15 min. The cells were washed twice with PBS buffer before being re-suspended in culture media (500 μL) and analysis was carried out on a Becton Dickinson FACS Aria flow cytometer. The average red fluorescence intensity (10,000 cells) was analyzed on the FL-2 channel when the TMRE red emissions decrease as the $\Delta\Psi_m$ decreases.

2.7.3. Analysis of autophagy by flow cytometry—Autophagy was detected using a Cyto-ID® autophagy detection kit (Enzo Life Science, Farmingdale, NY) using Cyto-ID™ green autophagy detection reagent, which selectively labels green vacuoles associated with the autophagy pathway, with minimal background lysosomal staining. Briefly, cells were harvested from culture and plated on a 24-well plate (7.0×10^4 cells per well) for 4 h in the presence or absence of 600 nM necrostatin-1. After incubation, the supernatant was discarded, and the cells were treated with complex **4** at different concentrations and incubated for various times at 37 °C in 5% CO_2. After incubation, the cells were washed with PBS buffer, centrifuged (1000 rpm for 5 min), and the supernatant was discarded. Following this, the cells were trypsinized, washed and re-suspended in fresh indicator-free DMEM containing 5% FBS. CYTO-ID Green stain solution was added before incubation for 30 min in the dark. Afterwards, the cells were washed, re-suspended in culture media, and fixed in 4% formaldehyde for 20 min. The samples were analyzed on a Becton Dickinson FACS Aria flow cytometer in the FL-1 and FL-2 channels. Autophagic activity was estimated measuring the mean fluorescence intensity (MFI) value. Positive controls for inducing autophagy included rapamycin (500 nM), chloroquine (120 μM), and starvation (DMEM-FBS). The results shown are representative of multiple experiments performed in triplicate.

3. Results and discussion

3.1. Synthesis and characterization

The MeATSC **1** ligand was synthesized and characterized as by Beckford et al. [140]. Complexes **2** and **3** were synthesized; then characterized by ^{1}H NMR spectroscopy (see Supplementary information for the ^{1}H NMR spectra for complexes **2** and **3**) as reported in the literature [153–155]. Scheme 1 shows the synthetic procedure for the formation of complex **4**.

Elemental analysis was carried out on complex **4**. The percentage for carbon, hydrogen, and nitrogen were found as 53.23%, 3.73%, and 14.14%, respectively, with the best fit being the complex with 1.5H_2O and ethanol as solvates. The percentage of hydrogen found in complex **4** was 3.73% versus the calculated value of 4.15%. The elemental analysis data for the percentage of H is not fully consistent with the calculated value, but other spectroscopic methods confirmed the identity and purity of complex **4**. Due to the fact that the discrepancy is only in the hydrogen, it is likely due to an error in the analysis process or the loss of ethanol and/or water as solvate(s) during the analytical procedure.

Another reason is based on the fact that there are some discrepancies in CHN data for some coordinated thiosemicarbazones as reported in some of the literature. We noticed these discrepancies in our previously reported data on vanadium(IV) complexes (with acetylethTSC and *N*-ethhymethohcarbthio ligands) [161] and the MeASTC ligand **1** as reported by Kate et al. [162], where their calculated %C was lower than the found %C for [Cu(ATSC)$_2$]; anal. calcd for $C_{32}H_{24}N_6S_2$ Cu: C, 61.2; H, 3.90; N, 13.54. Found: C, 59.79; H, 3.62; N, 13.48. We also believe that in our case and those discrepancies in the elemental analyses of complexes with thiosemicarbazones as reported by Sobiesiak et al. [163] (% calculated and found for H in dichlorido(1-[amino(thioxo)methyl]-5-hydroxy3-methyl-1H-pyrazole-κN^2)cobalt (II)), Lewis et al. [161], and Kate et al. [162], that tautomerism in thiosemicarbazones [140] could be occurring, hence causing the discrepancy in the %H in our case for complex **4**.

3.1.1. High resolution mass spectral analysis and conductivity measurements of complex 4—

High resolution mass spectra (HRMS) were acquired for complex **2**, [Co(phen)$_2$(O_2CO)]PF_6, **3**, and [Co(phen)$_2$(H_2O)$_2$](PF_6)$_3$, and complex **4** (see Figs. 1 and S1, Supplementary information for the HRMS for the respective cations). In all mass spectral analyses, M was assigned as the molecular ion minus any solvates.

For complex **2** and [Co(phen)$_2$(O_2CO)]PF_6, a species with the following formula was detected: $[C_{25}H_{16}CoN_4O_3]^+$, for $[M-Cl^-]^+$ and $[M-PF_6^-]^+$, respectively(see Fig. 1). In both cases, [Co(phen)$_2$(O_2CO)]$^+$ was formed in the mass spectrometer.

For complex **3** and [Co(phen)$_2$(H_2O)$_2$](PF_6)$_3$, species with the following formulas were detected: $[C_{24}H_{16}CoN_4O_2]^+$ (a peroxo complex, [Co(phen)$_2$(O_2)]$^+$), and $[C_{24}H_{18}CoN_4O_2]^+$ (a dihydroxo complex, [Co(phen)$_2$(OH)$_2$]$^+$, see Fig. 1). For complex **3**, the base peak for $[C_{24}H_{16}CoN_4O_2]^+$ occurred at m/z = 451.0599 ($[M-3NO_3^- - H_2 - 2H^+]^+$), where the

calculated m/z = 451.0600. For complex **3**, another base peak for $[C_{24}H_{18}CoN_4O_2]^+$ occurred at m/z = 453.075, where the calculated m/z = 453.0756 ($[M-3NO_3^- -2H^+]^+$).

The m/z value of 355.5798 which is detected for the cobalt(III)-containing species arising from complex **4** suggests that in addition to the loss of the three NO_3^- counter ions, tautomerization of the ligand, MeATCS **1** (Figs. 1, S1, and Schemes 2 and 3) [140], and deprotonation of the thiolate anion occurs upon coordination to the cobalt(III) metal center. The results obtained are in agreement with the expected structural formula for complex **4** and the cation formed in the mass spectrometer as shown in Schemes 1 and 3, respectively. Hence, the species detected is doubly charged as shown in Scheme 3, where the calculated exact mass of the doubly charged cation = 711.1604 g mol^{-1} (see Fig. 1 for the high resolution ESI mass spectrum of the cationic species formed).

Fig. S1 shows the HRMS of the cations formed from complex **4** and the proposed structure of the $[Co(phen)_2]^+$ species with a found m/z = 419.0693 (calculated m/z = 419.0701), which is believed to be formed from the loss of three NO_3^- counterions and the MeATSC **1** ligand, followed by an intramolecular electron transfer (or autoreduction) of one electron from each of the phen ligands to reduce the cobalt (III) metal center to form a cobalt(I) metal center.

To the best of our knowledge, this is the first report of its kind in the literature. However, there are reports of autoreduction of cobalt catalysts supported on carbon nanotubes and carbon spheres, nitrogen-doped carbon spheres, and cobalt nanoparticles supported on ordered mesoporous carbon for the Fischer-Tropsch synthesis [164–166]. Another example of autoreduction of cobalt-containing species is based on the effect of nitrogen on the autoreduction of cobalt nanoparticles supported on nitrogendoped ordered mesoporous carbon for the Fischer-Tropsch synthesis [167]. Also autoreduction of Pd-Co and Pt-Co cyanogels, where the cyanide ligand acts as a reducing agent and reduces the metal centers to lower oxidation states [168].

Autoreduction of some copper(II)-containing species is also known to occur as reported in the literature [169–173]. Autoreduction of bischelated copper(II) complexes of 6,6′-dialkyl-2,2′-bipyridines [169] and 8-dimethylarsinoquinoline [174] has also been reported. In those papers, the reduction of copper(II) is not attributed to the donor atoms of the ligands (i.e., the electronic properties) but to the geometry of a complex, which is exclusively defined by the sterically hindered group of a ligand [169,174]. Thus, upon the control of the geometry of a complex, which prefers Cu(I) to Cu(II), the reduction of copper(II) complexes to copper(I) complexes occurs [169,174].

Another example is where intramolecular electron transfer in Cu(II) complexes with aryl-imidazo-1,10-phenanthroline derivatives [175], where the observed autoreduction of Cu(II) to Cu(I) was explained by at least three reasons. These were as follows: (1) the presence of donor substituent in the phenyl ring of the ligand, phenyl (1), 4-(*N*,*N*-dimethylamino)phenyl, (2) the geometry around the copper(II) metal center, and (3) the solvent effect [175].

Conductivity measurements were carried out on a 1.0 mM solution of complex **4** in CH_3CN. It was determined that Λm = 295 Ω^{-1} cm^{-1} mol^{-1} which proved the existence of complex **4**

as a 2:1 electrolyte (providing two NO_3^- anions and one $[Co(phen)_2(MeATSC)]^{2+}$ cation) based on the use of conductivity measurements to ascertain types of electrolytes in various solvents as reported in a review as written by Geary [176] (where a summary of the expected Λ_m ranges for complexes of different electrolyte types at 10^{-3} M in the common solvents solvent, including CH_3CN (Ω^{-1} cm^{-1} mol^{-1}) is shown in Table 11 of this citation of Geary) [176]. It was also found that Λ_m = 72 Ω^{-1} cm^{-1} mol^{-1} in DMSO, which is a very important piece of data to add to the compilations of Geary [176].

Complex **4** as a 2:1 electrolyte accounts for the presence of a mononuclear dication ($[Co(phen)_2(MeATSC)]^{2+}$) in CH_3CN [176], which complements the mass spectral data for the doubly charged cation in the mass spectrometer, where MeATSC **1** is coordinated as a thiolate after tautomerism [140] (see Scheme 3).

3.1.2. FTIR spectroscopic analysis of the “free” ligand and complex 4—

Thiosemicarbazones exhibit characteristic stretching frequencies in specific energy regions as “free” ligands as well as coordinated ligands [140,161,177]. Thiosemicarbazones are able to coordinate to a metal center either as thione (neutral) or thiolate (anionic) ligands [140,161,177,178]. The hydrazinic N(2)–H stretching frequency (Scheme 2), which is initially observed at 3200 cm^{-1} for the ligand, was observed at 3053 cm^{-1} in complex **4**. This hydrazinic stretching frequency is confirmation that the ligand is coordinated as the thione and not the thiolate while complex **4** is in the solid state. The thiocarbonyl group of the MeATSC **1** ligand exhibited stretching frequencies at 841 cm^{-1} and 1254 cm^{-1}. The FTIR spectrum of complex **4** showed stretching frequencies for the C═S bond at 827 cm^{-1} and 1224 cm^{-1}.

In the FTIR spectra of the “free” ligand, MeATSC **1** and complex **4** (Fig. S2 and Table 1), the N(1)–H stretching frequency was observed at 3397 cm^{-1} for the “free” ligand, while it was shifted to a lower stretching frequency of 3227 cm^{-1} when the ligand was coordinated to the cobalt(III) metal center. A similar trend occurred for [VO(sal-*L*-tryp) (MeATSC)] $\cdot 1.5C_2H_5OH$ [161] (see Table 1). Similarly, the ν(C═N) stretching frequency was observed at 1580 cm^{-1} for complex **4**, which is a lower stretching frequency when compared to the “free” ligand at 1620 cm^{-1}. The relatively slight shift of 40 cm^{-1} for the ν(C═N) stretching frequency from a “free” ligand to a coordinated ligand indicates that the imine’s nitrogen atom is involved in coordination to the cobalt(III) metal center. This trend of a decreased ν(C═N) stretching frequency upon complexation of the “free” ligand to a metal center was also observed by Beckford et al. [140] for analogous ruthenium(II) complexes, $[(bpy)_2Ru(MeATSC)](PF_6)_2$ and $[(phen)_2Ru(MeATSC)](PF_6)_2$ with the coordinated MeATSC **1** ligand. Finally, the stretching frequency for the NO_3^- counter ions is observed at 1323 cm^{-1} which is similar to what is typically observed for the “free” nitrate anions as reported in literature [179,180].

3.1.3. UV–visible spectroscopic analysis of the “free” ligand 1, $[Co(phen)_2(O_2CO)]PF_6$, $[Co(phen)_2(H_2O)_2](PF_6)_3$, and complex 4—

The UV–visible spectra of $[Co(phen)_2(O_2CO)]PF_6$ and $[Co(phen)_2(H_2O)_2](PF_6)_3$ were acquired in DMSO (Fig. 2). The UV–visible spectrum of complex **4** was also acquired in DMSO (Fig. 2), where four wavelengths were observed at 264, 355, 372, and 392 nm with molar extinction

coefficients of 8.9×10^4, 0.85×10^4, 0.93×10^4, and 1.0×10^4 M^{-1} cm^{-1}, respectively (see Fig. 2). These three spectra were acquired to show the differences in each spectrum on changing the coordinated ligands, viz., CO_3^{2-}, H_2O, and MeATSC **1**.

Table 2 shows the UV–visible spectroscopic data for the respective species in DMSO. Clearly there are some differences, where the d-d transitions for $[Co(phen)_2(O_2CO)]PF_6$ and $[Co(phen)_2(H_2O)_2](PF_6)_3$ occur at 502 and 513 nm, respectively.

On comparing the spectrum of complex **4** to the spectra of the MeATSC **1** ligand, $[Co(phen)_2(O_2CO)]PF_6$, and $[Co(phen)_2(H_2O)_2]$ $(PF_6)_3$, it is clear that 264, 355, 372, and 392 nm are from the anthracene moiety of the ligand. The most striking feature of these spectra is the broadening of the vibrational structure in the region of anthracene absorption together with a clear blue-shift with respect to the MeATSC ligand. The d–d transition of the cobalt(III) metal center (compared to the molar extinction coefficients for $[Co(phen)_2(O_2CO)]$ PF_6, and $[Co(phen)_2(H_2O)_2](PF_6)_3$ are 126 and 186 M^{-1} cm^{-1} at 502 and 513 nm, respectively) is hidden in the spectrum for complex **4** because of the broadening of the anthracene bands that tail off into the visible region.

Fig. S3 shows the UV–visible spectra of complex **4** in DMSO, H_2O, and CH_3CN, where the spectral profiles are similar with respect to the presence of the anthracene moiety in MeATSC **1**.

3.1.4. ^1H, ^{13}C, and ^{59}Co NMR spectroscopic analysis of the "free" ligand and complexes 2–4—

^1H and ^{13}C NMR spectra were acquired for the "free" MeATSC ligand **1** and complexes **2**–**4** (Figs. 3–4 and S4), where appropriate. The ^1H NMR spectrum of the "free" MeATSC **1** ligand was previously reported [140], but we will discuss its NMR spectroscopic features and compare them with the coordinated ligand, MeATSC **1**.

Complex **2** was characterized via ^1H NMR spectroscopy where it was compared to what was observed in literature [154]. Once complex 2 was determined to be pure, acid hydrolysis was carried out to produce complex **3**. The product's ^1H NMR spectrum was compared to the chemical shifts in the literature; where complex **3** was proven to be pure [155]. ^1H NMR spectra of complexes **2** and **3** are shown in Fig. S4, where the aromatic protons that were overlapping circa 7.5 ppm in complex **2** are no longer overlapping in complex **3**.

The ^1H NMR chemical shift for the methyl group of complex **4** occurred at 3.13 ppm and this is consistent with the previously observed ^1H NMR chemical shifts for the MeATSC **1** moiety [140]. Upon coordination to the cobalt(III) metal center, the chemical shift for the imine linkage (H–C═N) was observed between 7.50 and 8.72 ppm (Fig. 4) as reported in the literature [181,182], and the chemical shift resulting from H-N(3) as labelled in a typical thiosemicarbazone shifted upfield by 2 ppm when coordinated to the cobalt(III) metal center. Due to the overlapping of the aromatic protons, the aromatic protons from MeATSC **1**, were identified from the ^1H-^1H COSY NMR spectrum, Fig. S9. The aromatic protons for the MeATSC ligand in complex **4** were observed at 7.49 (d), 7.75 (e), 8.06 (c), 8.52 (h), and 8.94 (f) ppm (see Fig. 4). When comparing the "free" ligand protons, the chemical shifts that correspond to c (8.14 ppm) and h (9.28 ppm) were shifted upfield when coordinated to the

metal center and the proton that corresponds to f (8.50 ppm) was shifted upfield. The hydrazinic proton H–N(2) which occurred at 11.7 ppm for the “free” ligand was shifted upfield to 10.1 ppm upon coordination to the cobalt(III) metal center [182,183]. The signal integrations and multiplicities agreed with the proposed structural formula of complex **4**. The ethanol solvate was detected at the following chemical shifts: 1.07 (a triplet) and 3.44 ppm in the ^{1}H NMR spectrum, and at 19.01 and 56.49 ppm for the ^{13}C NMR spectrum (see Fig. 4).

In the ^{13}C NMR spectrum (Fig. 3), the chemical shift for the thione (C═S), which was observed at 178 ppm in the “free” ligand, MeATSC **1**, was hardly observed for complex **4** at 172 ppm (Fig. 4). The low intensity of the chemical shift suggests that when dissolved in solution, the complex undergoes tautomerization and is in an equilibrium that may favor the predominance of the thiolate over that of the thione. The chemical shift of the methyl group was observed at 31 ppm when MeATSC **1** is coordinated to the cobalt(III) metal center. The C(1)═N chemical shift was observed to be shifted slightly upfield to 141 ppm in complex **4** from 142 ppm in the “free” ligand, MeATSC **1**, a trend which is comparable to what occurred in the literature when MeATSC **1** is coordinated to a metal center [140,182]. The aromatic chemical shifts of the “free” ligand were observed from 120 to 130 ppm. The aromatic chemical shifts for carbons d, e, c, and h were observed at 125.37, 128.86, 128.33, and 129.25 ppm, respectively. These carbons were identified from the ^{1}H chemical shifts in the ^{1}H-^{13}C HSQC NMR spectrum (Fig. S10).

In terms of the metal center in complex **4**, transition metal NMR chemical shifts are useful probes of the structure and reactivity of many coordination complexes since those chemical shifts allow for tiny variations at the coordination metal center under investigation [184]. It is known that the isotope ^{59}Co exhibits the largest known shielding range, spanning some 18,000 ppm or more [185–187]. It is also 100% naturally abundant, possesses a relatively high magnetogyric ratio [188], and by virtue of the magnetic mixing of its occupied and excited d orbitals, it may experience substantial paramagnetic deshielding (> 15,000 ppm) that will reveal subtle changes in the chemical environment of a cobalt metal center [187,188]. Recently, we reported a ^{59}Co NMR spectroscopic study on $[Co(dmgBF_2)_2(H_2O)_2]$ and $[Ru(pbt)_2(L\text{-}pyr)Co(dmgBF_2)_2(H_2O)](PF_6)_2\cdot 11H_2O\cdot 1.5CH_3COCH_3$, while comparing the resulting chemical shifts with analogous cobalt(II)-containing complexes [189]. The ^{59}Co NMR spectrum for $[Co(dmgBF_2)_2(H_2O)_2]$ occurs at $\delta = 5652$ ppm and at $\delta = 5401$ ppm for $Ru(pbt)_2(L\text{-}pyr)Co(dmgBF_2)_2(H_2O)](PF_6)_2\cdot 11H_2O\cdot 1.5CH_3COCH_3$ with DMSO−d_6 as solvent [189].

In our current study, ^{59}Co NMR spectra were also acquired for $[Co(phen)_2(O_2CO)]PF_6$, $[Co(phen)_2(H_2O)_2](PF_6)_3$, and complex **4** in DMSO−d_6, where chemical shifts were observed at 8362, 7070, and 7067 ppm for $[[Co(phen)_2(O_2CO)]PF_6$, $[Co(phen)_2(H_2O)_2](PF_6)_3$, and complex **4**, respectively (Figs. 5 and S11, Supplementary information). Table S1 shows the respective chemical shifts of our complexes and selected cobalt(III) complexes (also the first report of a ^{59}Co NMR spectrum of one cobalt(I) species that was reported by our laboratory, viz., $[^{n}Bu_4N][Co(bpy)_2(solv)]$ [190] (where solv = H_2O and/or CH_3CN) generated in situ from $[Co(bpy)_2Cl_2]$ in the presence of 10 equivalents of $[^{n}Bu_4N]BH_4$ in CD_3CN-D_2O (4:1, v/v) at 28 °C) that are reported in the literature. The chemical shift for

$[Co(phen)_2(O_2CO)]PF_6$ occurs at δ_{Co} = 8362 ppm, which is within the range 7965–10,121 ppm for all of the selected carbonate complexes with a cobalt(III) metal center as shown in Table S1.

It is interesting to note that $[Co(phen)_2(H_2O)_2](PF_6)_3$ and complex **4** have very close chemical shifts (δ_{Co} = 7070 and 7067 ppm, respectively), but $[Co(phen)_2(O_2CO)]PF_6$ has a chemical shift at δ_{Co} = 8362 ppm. From these ^{59}Co NMR spectra, it is evident that the ligand structure has a small effect on their relative ^{59}Co NMR chemical shifts, which fall within a range of ca 3 ppm of each other for $[Co\ (phen)_2(H_2O)_2](PF_6)_3$ and complex **4**. The huge difference between the chemical shift of $[Co(phen)_2(O_2CO)]PF_6$ and those of $Co(phen)_2(H_2O)_2]\ (PF_6)_3$ and complex **4** is probably due to the ligand field strength [191] (and the correlation between the spectrochemical series and ^{59}Co NMR spectra [192–195]) of the ligands in the three complexes. For $[Co(NH_3)_6]^{3+}$ and $[Co(NH_3)_5(H_2O)]^{3+}$, δ_{Co} = 8160 and 9060 ppm, respectively [193]. Here $H_2O < NH_3$ in the spectrochemical series, and for our compounds, we can imply that $CO_3^{2-} < H_2O \approx$ MeATSC.

3.2. UV–visible and spectroscopic studies (in water, PBS buffer, and an aqueous solution of reduced glutathione) and interaction with ctDNA

3.2.1. Spectroscopic studies in water, PBS buffer, and an aqueous solution of reduced glutathione; and ctDNA binding studies—

The investigation of the binding of metal complexes to DNA is of prime importance in the development of anti-cancer drugs [196]. From a pharmacological point of view, the primary target of many anti-cancer drugs is DNA [36–45]. Consequently, DNA binding activities of metal complexes have often been a key parameter during the development of chemotherapeutic drugs. Therefore, the extent of binding of complex **4** to ctDNA was ascertained via UV–visible spectroscopic studies.

Before such studies were conducted, stability studies in water, PBS buffer, and a PBS buffered solution of reduced glutathione (GSH) were carried out. Here the absorbance at the high-energy absorption band in complex **4** was monitored over 24 h (Figs. S12–S14, Supplementary information). The stability of the complex was monitored for one week in water (Fig. S12), PBS buffer solution (Fig. S13), and in a PBS buffered solution of GSH (Fig. S14). The stability of the complex in each solution was characterized by the peak area remaining of the starting complex.

After the first 24 h of mixing the reduced glutathione solution with complex **4** (Fig. S14), the absorbance change is larger when compared to the complex in either PBS buffer or water. Clearly there is an appreciable reaction occurring between GSH and complex **4**. The first order rate constants, k, were calculated as $2.5 \times 10^{-6}\ s^{-1}$ ($8.9 \times 10^{-3}\ h^{-1}$), $5.6 \times 10^{-6}\ s^{-1}$ ($2.0 \times 10^{-2}\ h^{-1}$), and $1.3 \times 10^{-5}\ s^{-1}$ ($4.7 \times 10^{-2}\ h^{-1}$) in H_2O, PBS buffer, and reduced glutathione in PBS buffer, respectively.

Metal complexes of reduced glutathione (GSH) serve important functions in biological systems and play a dominant role in protein metabolism. These are important constituents of enzymes, proteins and present in many parts of the biological system [197]. Reduced glutathione is the most important cellular thiol which exists in mammalian cells and creates

in the cell an important redox system [198–200]. It exists in the concentration range. 0.1–10 mM and is readily oxidized to the disulfide (GSSG) [197].

In the literature, the reactions of the pentaamminechromato cobalt (III) complex cation, $[Co^{III}(NH_3)_5OCr^{VI}O_3]^+$, with a series of thiols, RSH (where RSH = reduced glutathione, *L*-cysteine, and *D,L*-penicillamine) was studied by spectrophotometry at pH > 7, over the range 20 °C ≤ *T* ≤ 34.4 °C, with the thiols in excess at ionic strength 0.50 M ($NaClO_4$) at pH 7.4 [201]. The reactions occurred in two stages; the first was a rapid reaction between reactants leading to formation of outer-sphere adducts, which were facilitated by electrostatic interaction between the chromato complex and each thiol [201]. In the study, the pentaamminecobalt(III) moiety was not reduced, but reacted slowly with the thiols to form complexes. These latter complexation reactions were significantly slower than the electron transfer reactions [201]. In another study, the reduction of the cobalt(III) complex, $[Co^{III}(HL)]\cdot 9H_2O$ (where H4L = 1,8-bis(2-hydroxybenzamido)-3,6-diazaoctane) by GSH was studied by conventional spectrophotometry in acidic media [202]. The final products were determined to be the corresponding Co(II) complex and GSSG [202].

In our current study, there is the possibility of competing aquation and anation substitution reactions when GSH is reacted with complex **4**, but we can conclude that complex **4** is fairly stable in either water of PBS buffer over 72 h in the absence of GSH. We do know that a detailed study involving the reaction between GSH and complex **4** is warranted in the future.

Regarding studies involving ctDNA, there are reports in the literature, where complexes that intercalate into the DNA will generally show bathochromic and hypochromic changes relative to the “free” complex [203].

Hypochromism and bathochromism in the UV–visible spectrum following addition of ctDNA indicates the complex can interact with ctDNA, most likely through stacking interactions between an aromatic ring and the base pairs of ctDNA [203]. The extent of hypochromism is often an indicator of the strength of intercalation [203]. Qualitatively, the slight hypochromism observed indicates the weakness of this interaction [203].

From the UV–visible studies carried out on MeATSC **1**, and complexes **3** and **4**, as shown in Figs. S15, S16, and 6, respectively, ctDNA has a λ_{max} at 260 nm, ranging from about 225 to 300 nm, whereas the ligand and complexes used in this study also absorb within this region as well. Upon introduction of the ctDNA to MeATSC **1**, Fig. S15, the absorbance between 300 and 550 nm decreases (hypochromism) with each increase in ctDNA concentration. This was also observed with complex **4** within the same region, but to a lesser extent with complex **3** circa 352 nm.

With complex **3**, Fig. S16, a hyperchromic effect is observed at 272 nm which is similar to what is observed with the MeATSC **1** at 254 nm, but a hypsochromic shift of ~1 nm occurred at the highest concentration of ctDNA. The precision of the measurements using this technique was low. This is due to the fact the low absorbances recorded at ~355 nm makes it very difficult to determine an accurate K_b value. In summary, we could not obtain a binding constant for complex **3** even after multiple experiments.

For complex **4**, upon the addition of ctDNA, the absorbance bands exhibited hypochromism accompanied by a red shift (Fig. 6). Even though the studies with complex **4** (Fig. 6) show similar spectral characteristics as MeATSC **1** between 350 and 400 nm, an isosbestic point was observed at 420 nm on increasing ctDNA concentration.

In order to compare the DNA binding affinity of the MeATSC **1** ligand and complex **4**, the intrinsic binding constants, K_b, were determined using the following equation [98,204–207]:

$$\frac{[ctDNA]}{\varepsilon_a - \varepsilon_f} = \frac{[ctDNA]}{\varepsilon_b - \varepsilon_f} + \frac{1}{K_b(\varepsilon_b - \varepsilon_f)} \quad (1)$$

where ε_a is the molar extinction coefficiesnt (A_{obsd}/[complex](or) [MeATSC]) observed for the lowest energy absorption band at a given ctDNA concentration, ε_f is the molar extinction coefficient of the analyte in the absence of ctDNA, and ε_b is the extinction coefficient of the analyte fully bound to ctDNA. For the plots of [ctDNA]/($\varepsilon_a - \varepsilon_f$) versus [ctDNA], the K_b value is calculated from the ratio of the slope to the intercept [208,209]. The K_b values for MeATSC **1** and complex **4** were calculated to be 8.1×10^5 and 1.6×10^4 M^{-1}, respectively (see Figs. S15 and 6, respectively).

The results suggest that an appreciable intercalative mode of binding may be unlikely. A small amount of intercalation in the case of MeATSC **1** and complex **4** may be possible because of steric demands. The larger steric demands of complex **4** probably thwarted stronger intercalation [210], but the reason for the apparent lack of greater surface binding is not clear. It is possible that the shape of the complex **4** prevents binding on the surface of ctDNA. Another reason could be that it is possible that in aqueous solution, $([Co(phen)_2(MeATSC)]^{2+}$ could be the active species binding to ctDNA (complex **4** could be a 2:1 electrolyte in water, while extrapolating the conductivity measurements in CH_3CN as mentioned above and the use of data as cited by Geary [176]). This could account for the low binding as a result of a mononuclear dication ($[Co(phen)_2(MeATSC)]^{2+}$), not a mononuclear triication ($[Co(phen)_2(MeATSC)]^{3+}$). Over all, this could be due to the tautomerism of complex **4** in aqueous solution (see Scheme 2).

The calculated K_b values of MeATSC **1** and complex **4** shown in Table S2 seem to confirm that intercalation is not a major player in the binding of complex **4** to ctDNA. The K_b values were also compared to selected complexes and ATSC. The K_b value of 1.6×10^4 M^{-1} for complex **4** was comparable to the K_b values for the following complexes [211]: $[Co(phen)_2(pdtb)](ClO_4)_3$, $Co(phen)_2(pdta)](ClO_4)_3$, and $[Co\ (phen)_2(pdtp)](ClO_4)_3$, which were reported to be 0.862×10^4, 2.81×10^4, and 4.01×10^4 M^{-1}, respectively.

The observed binding constant also revealed that complex **4** interacts weakly with ctDNA when compared to ethidium bromide ($K_b = 1.4 \times 10^6$ M^{-1}) [212] and $[Ru(bpy)_2(dppz)]^{2+}$ ($K_b > 10^6$ M^{-1}) [213,214]. This suggests weak DNA binding because the extent of hypochromism is usually associated with the strength of DNA interaction as reported with the use of ruthenium(II)-containing complexes [215–217]. When compared to the K_b values of 38×10^4, 3.23×10^4, and 10.1×10^4 M^{-1}, for [Cu(ATSC)] [162], $[Ru(bpy)_2(ATSC)]$

$(PF_6)_{2[}140_{]}$, and $[Ru(phen)_2(ATSC)](PF_6)_2$ [140], respectively, our K_b value of 1.6×10^4 M^{-1} is smaller in magnitude.

Our co-worker Beckford [218] synthesized a set of three trinuclear complexes containing organometallic ruthenium fragments-(arene) RuCl coordinated to a 2,4,6-tris(di-2-pyridylamino)-1,3,5-triazine core [(arene = benzene, *p*-cymene, or hexamethylbenzene]. The interaction of the complexes with ctDNA was extensively studied using a variety of biophysical probes as well as by molecular docking [218]. The complexes as reported by Beckford et al. [218] bind strongly to ctDNA with apparent binding constants ranging from 2.20×10^4 to 4.79×10^4 M^{-1}. Similar to studies here, the mode of binding to the nucleic acid was not definitively determined, but the evidence pointed to certain non-specific electrostatic interaction [218]. It must be cautioned, as mentioned in the literature by Turro and co-workers [219], since the optical changes of the probe in the presence of DNA are not likely to be a result of a 1:1 complex/base interaction, fits that assume such a binding model may not be useful for obtaining accurate DNA binding constants for complexes that may exhibit aggregation in water and/or on the DNA surface [219]. This may be the case for MeATSC **1** and complex **4**. On the other hand, we will carry out complementary competitive binding between ethidium bromide (EB) and MeATSC **1** and complexes **3** and **4** for ctDNA.

In order to investigate the interaction mode between the complexes and ctDNA, the EB fluorescence displacement experiment will be employed [220]. EB is a planar cationic dye that is widely used as a sensitive fluorescence probe for native DNA. EB emits intense fluorescent light in the presence of DNA due to its strong intercalation between the adjacent DNA base pairs. The displacement technique is based on the decrease of this fluorescence resulting from the displacement of EB from a DNA sequence by a quencher [220]. The quenching is due to the reduction of the number of binding sites on the DNA that is available to the EB. The method will therefore provide indirect evidence for an intercalative binding mode. The extent of fluorescence quenching may also be used to determine the extent of binding between the quencher and DNA.

Given the indeterminacy of the results from the electronic absorption studies with respect to a mode of binding, future studies with these analytes and the use of isothermal titration calorimetry (ITC) [221] will be carried out to complement the studies mentioned above. When studying the binding interactions between a ligand and a macromolecule, ITC has many advantages. It is a powerful, high-precision tool that is often referred to as the “gold standard” for quantitative measurements of biomolecular interactions, and the only direct thermodynamic method that enables full thermodynamic characterization (stoichiometry, association constant, enthalpy and entropy of binding) of the interaction after a single titration experiment [221–225].

3.3. Topoisomerase inhibition studies

Topoisomerases are ubiquitous enzymes, found in all kingdoms of life. They are required for untangling DNA and restoring the native DNA topology after many cellular processes such as replication, transcription, as well as other events that perturb the DNA topology [226]. Their enzymatic activities are therefore essential for cell viability. Topoisomerase enzymes use an active site tyrosine residue to attack the phosphodiester backbone of the DNA, which

causes the strand to break. The enzyme then passes or rotates a second strand(s) through or around the break, re-ligates the DNA break, and releases the DNA product with altered topology [226,227]. Topoisomerases can either cut one strand of DNA (Type I) or both strands (Type II) [228]. An important feature of the general mechanism is the ensuing covalent intermediate: while the DNA strand is broken, the enzyme is covalently linked to it. As long as the covalent intermediate persists, the cell is in danger, as accumulation of DNA breaks can cause DNA damage response in cells, and even apoptosis [227,228].

Fig. 7A shows the activity of human topoisomerase I (hTOP1) in the presence of varying concentrations of complex **4** and MeATSC **1**. Complex **4** showed excellent inhibition of hTOP1 relaxation activity at low concentrations. Importantly, the ligand, MeATSC **1** and the precursor (complex **3**) to complex **4** showed no significant inhibition of the enzyme. The IC_{50} value (IC_{50} is defined here as compound concentration for the DNA to have electrophoretic mobility half way between fully supercoiled and fully relaxed) for $[Co(phen)_2(H_2O)_2](NO_3)_3$ **3** is > 100 μM, for MeATSC **1** is 50 μM, and for complex **4** is between 3 and 6.4μM.

Fig. 7B shows the effect of the complex on human topoisomerase IIα (hTOP2α) in the presence of the complex and its ligand. Complex **4** also showed good activity for the inhibition of hTOP2α, albeit requiring higher concentration. As with the type I enzyme, the complex alone displayed significant inhibition with calculated IC_{50} values for both $[Co(phen)_2(H_2O)_2](NO_3)_3$ **3** and MeATSC **1** are > 100 μM, and for complex **4** is 25.5 μM. The greater sensitivity of hTOP1 versus hTOP2α suggested that the inhibition of DNA relaxation by hTOP1 observed for complex **4** is not due solely to DNA intercalation. DNA was relaxed nearly completely by hTOP2α in the presence of 12.7 μM complex **4** (lanes 14, Fig. 7B) so this concentration of complex **4** does not result in significant DNA intercalation. In contrast, the DNA remained fully supercoiled in the presence 12.7 μM complex **4** in the hTOP1 reaction (lane 15, Fig. 7A), demonstrating that the hTOP1 relaxation activity is inhibited totally at this complex **4** concentration.

Topoisomerase inhibitors can fall into two categories, viz., catalytic inhibitors and poison inhibitors [229,230]. Catalytic inhibitors prevent the enzyme from working entirely, while topoisomerase poisons stabilize the covalent intermediate to prevent DNA re-ligation. Both types of inhibition can be effective at killing cancer cells [229,230]. To determine whether complex **4** acts as a poison inhibitor, cleavage products were analyzed by agarose gel electrophoresis in the presence of ethidium bromide to allow for the separation of nicked or linear DNA from covalently closed relaxed DNA. In the presence of a poison inhibitor, the amount of cleaved DNA product would increase. As shown in Fig. 8, the addition of complex **4** did not increase the amount of nicked or linear DNA products formed from hTOP1 (Fig. 8A) or hTOP2α (Fig. 8B), suggesting that complex **4** is a catalytic inhibitor. In fact, at a concentration of 50.9 μM, complex **4** caused a decrease in the amount of linear DNA product from hTOP2α as compared to the DMSO control. This indicates inhibition of either DNA binding or DNA cleavage.

3.4. Cytotoxicity evaluation

The cytotoxicity of the compound against a model metastatic breast cancer cell line 4T1-luc was determined by means of the MTS (a colorimetric) assay, which serves as an index of cell viability by detecting the reduction of a tetrazolium compound to a purple formazan product in the presents of NADPH or NADH produced by dehydrogenase enzymes in metabolically active cells. 4T1-luc cells were treated with increasing concentrations of complex **4** for 24 h, and the viability was measured by the MTS assay. Cells were seeded at 2.5×10^4 cells per well for 24 h prior to addition of increasing concentrations of complex **4**. Complex **4** decreases 4T1-luc cell viability in a concentration-dependent manner after a 24 h treatment. An IC_{50} value of 34.4 ± 5.2 μM was calculated for complex **4** (Fig. 9).

For comparison, the IC_{50} value for cisplatin was 13.75 ± 1.08 μM. In comparison, the free MeATSC ligand **1** showed no significant growth inhibition at similar concentrations, which indicates that chelation of the ligand to the cobalt(III) metal center is necessary for the anti-cancer activity of complex **4**.

3.5. Cell death mechanism evaluations

3.5.1. Role of autophagy/necrosis signaling pathway in complex induced cell death—Autophagy is a conserved process of cellular degeneration in eukaryotic cells, in which unfolded, aggregated, or long-lived cytoplasmic proteins are delivered to the lysosome for degradation [231]. Under “normal” conditions, autophagy remains at low levels for maintenance of cellular homeostasis. However, autophagy is readily induced in response to nutrient deprivation, metabolic stress, radiation, anti-cancer drugs, endoplasmic reticulum (ER) stress, and/or increases in reactive oxygen species [232]. The ability of complex **4** to induce autophagy flux is shown in Fig. 10.

In Fig. 10A after 24 h of treatment, the mean fluorescent intensity of cells treated with 5 μM and 10 μM are significantly increased compared to unstained cells and untreated cells, thus indicating the presence of the autophagosome and other organelles associated with the induction of the autophagy process. At 80 μM there is a decrease in the mean fluorescence intensity indicative of the absence of the organelles associated with autophagy. This is most likely due to massive cell death at this time point. This is also evidence in Fig. 10B showing that autophagy only occurs at low complex concentrations 24 h after treatment. However, Fig. 11 showing time-dependent effects of 5 μM (panel A) and 80 μM (panel B), indicating that autophagy can be seen at high complex concentrations, but only at earlier times. The starvation is a positive control (red bar at 0 μM complex **4**), which is a signal for autophagy [233,234].

When cells are starved, they undergo autophagy to survive [233,234]. This finding is not uncommon as it is known that autophagy is primarily induced as a protective mechanism depending on the extent and duration of the treatment [235].

The regulatory event(s) that switch autophagy from a protective event to a cell death mechanism is (are) poorly defined. As shown in Fig. 11B, it is possible to inhibit autophagy

by utilizing necrostatin-1 at low concentrations (> 40 μM complex **4**); however, at higher concentrations of complex **4**, the protective nature of this inhibition is overcome.

In order to determine the role of autophagy in the complex-induced cell death, viability was determined in the presence and absence of necrostatin-1 (Fig. 12). In the presence of necrostatin-1, the viability curve for complex-induced cell death was shifted to the left, requiring lower concentrations to induce cell death. A comparison of the IC_{50} values in the absence or presence of necrostatin-1 shows a difference of about 10 μM, indicating that inhibition of autophagy enhances efficacy of complex **4**. This suggests that autophagy may provide some survival advantages of 4T1-luc cells in response to complex **4**. So, regardless of the different time and concentration effects of complex **4** on autophagy, at the 600 nM necrostatin concentration, inhibition of autophagy improved complex **4** toxicity on 4T1-luc cells as indicated by slightly lowering its IC_{50} value.

3.5.2. Role of caspase-3 in complex induced apoptosis in 4T1-luc cells—To determine if regulated cell death was due to apoptosis, we determined molecular events initiated by complex **4**, by monitoring the activity of executioner capsases-3 and −7. Fig. 13A shows complex **4** induces caspase-3/7 cleavage in a concentration dependent manner with peak activities occurring at four (4) h. Furthermore, preincubation with the pan caspase inhibitor z-VAD-FMK nearly completely inhibited caspase 3/7 activity at all concentrations.

To determine if caspase activation had an effect on cell viability, we assayed cell viability in the presence and absence of the pan caspase inhibitor z-VAD-FMK. As shown in Fig. 13B, the presence of z-VAD-FMK, loss of cell viability shifted to higher concentrations of complex **4** with the calculated IC_{50} value for the complex almost doubling to 64.6 ± 4.7 μM. This data indicates that complex **4** induces a caspase-dependent, apoptotic cell death. While we did not monitor upstream effector caspases (i.e., caspase 8 and caspase 9) and other apoptotic proteins (i.e., BAX, Bcl-2, BAD, BID), we definitively suggest that apoptosis stems from the extrinsic or intrinsic pathways; however, given that complex **4** interacts with DNA, it is possible that apoptosis is induced, at least in part, through the intrinsic pathway following DNA damage.

3.5.3. Modulation of the mitochondrial transmembrane potential ($\Delta\Psi_m$) TMRE retention—Mitochondria are often described as an essential target for cancer chemotherapy as they play a critical role in the regulation of cell fate by integrating cellular metabolism and apoptotic signals that originate both from intrinsic and extrinsic pathways [236–238]. Disruptions in mitochondrial-mediated events often lead to increases in caspase-3 activity [239]. Under normal conditions, the integrity of the outer mitochondrial membrane (OMM) is protected by Bcl-2 anti-apoptotic protein family (BCL-2, BCL-xL). To induce apoptosis, Bcl-2 pro-apoptotic effector proteins (BAX or BAK) must change conformations, oligomerize and insert into OMM to form pores that release proteins from the inner mitochondrial space, such as cytochrome *c*, which leads to caspase activation and apoptosis. A third subgroup of Bcl-2 family members, BH3 only proteins, can bind to both anti- and pro-apoptotic members. This leads to two apoptotic signaling mechanisms.

One or more upstream pro-apoptotic events are activated, and anti-apoptotic events are inactivated such that pro-apoptotic proteins BAX/BAK ultimately permeabilize the OMM [240]. Therefore, the ability of complex **4** to modulate the mitochondrial membrane potential ($\Delta\Psi_m$) was investigated via flow cytometric analysis. As observed in Fig. 14A, there are two distinct cell populations prior to treatment with approximately 83% of cells exhibiting a higher membrane potential (upper left quadrant) and 17% with a lower membrane potential (lower left quadrant). After 2 h of incubation with complex **4**, there is a concentration-dependent increase in the number of cells with a low membrane potential beginning at 40 μM and a maximum of 47% of cells exhibiting a lower membrane potential at the highest concentration tested (Fig. 14B–F).

Table 3 shows a dose-response and time course for complex **4** effects on the 4T1-luc cells' $\Delta\Psi_m$. The results are complex because the cell population is heterogeneous and there is a heterogeneity of their responses to complex **4** depending on the drug concentration. At the two (2) hour time point, there is a clear dose-dependent decrease in the $\Delta\Psi_m$, such that at 80 μM about half of the cell population has lost their MMP. The four (4) hour time point shows that cells exposed to 5–60 μM concentrations now have a greater loss of $\Delta\Psi_m$ compared to the two (2) hour time point, because complex **4** took longer to affect the MMP at these concentrations. However, at 80 μM, cells from the two (2) hour effect have essentially died and remaining cells have not responded at all to complex **4**, yet. However, by the six (6) hour time point, about half of the four (4) hour cells treated with 80 μM complex **4** have now lost their $\Delta\Psi_m$. Similar arguments can be made as lower complex **4** concentrations take longer to affect a heterogeneous cell population. 4T1-luc cells are known to be highly heterogeneous regarding genetic profiles [241] and effects of chemotherapeutic drugs [242]. Thus, it is not unexpected that 4T1-luc cells have different levels of sensitivity to complex **4** with higher concentration affecting some cells rapidly (2 h) and affecting a more resistant population later (6 h).

Based on evidence presented here, it is not exactly clear how the complex **4** initiates apoptosis. While it is possible that the complex could induce Fas ligand expression, which would have an autocrine effect to induce apoptosis through Fas death receptor, this is unlikely. Given that complex **4** binds to DNA, inhibits topoisomerases and results in dissipation of $\Delta\Psi_m$, it is much more likely that intrinsic apoptosis pathways are activated. For example, DNA damage and/or perturbation of mitochondria could involve p53-mediated transcription of pro-apoptotic proteins to induce OMM permeabilization as a typical intrinsic apoptosis mechanism [240,243]. It is also possible that complex **4** could result in a heavy metal or xenobiotic stress that would lead to intrinsic mechanisms to apoptosis induction.

4. Conclusions

In this study, we investigated the interactions of MeATSC **1**, complex **3**, and complex **4** with ctDNA. We also analyzed the biochemical effects of complex **4** on a model breast cancer cell line, 4T1-luc. Spectroscopic characterization showed complex **4** to contain the thiosemicarbazone in the thione isomeric form. However, there is tautomerization of the coordinated MeATSC ligand **1** on the cobalt(III) metal center within the mass spectrometer chamber and from conductivity measurements (where there was the formation of [Co

$(phen)_2(MeATSC)]^{2+}$ in CH_3CN). UV–visible spectroscopic studies indicate that complex **4** interacts with ctDNA in a weak intercalative fashion. While only weak interactions were observed with ctDNA, complex **4** showed good inhibition of human topoisomerase I and IIα.

Complex **4** showed moderate cytotoxic properties against 4T1-luc cells, whereas the “free” ligand, MeATSC **1** displayed no significant growth inhibition. Complex **4** was shown to induce apoptosis and dissipation of the mitochondrial membrane potential, $\Delta\Psi_m$. The potential mechanism for apoptosis induction is activation of the intrinsic mitochondrial apoptotic signaling pathway owing to the activation of caspase 3/7 and modulation of the $\Delta\Psi_m$. While complex **4** was shown to induce autophagy, as an initial survival mechanism, inhibition of autophagy and necroptosis signaling pathways did not have a large effect on the observed cell death, indicating their role in regulated cell death was relatively minor following exposure to complex **4**. Nevertheless, the attenuation of 4T1-luc cell viability in the presence of the caspase inhibitor z-VAD-FMK demonstrates a significant caspase-dependent component to cell death. The data presented from our study suggest that cobalt(III) complexes deserve further investigation as anti-cancer drugs. Further detailed mechanistic investigations on complex **4** as well as complexes bearing other thiosemicarbazone and structurally related ligands are currently underway.

Supplementary Material

Refer to Web version on PubMed Central for supplementary material.

Acknowledgements

AAH’s work to generate compounds **1**–**4** used in this study was supported by the Mississippi INBRE (P20RR016476), funded by the National Center for Research Resources, National Institutes of Health (NIH). AAH would like to thank the National Science Foundation (NSF) for the NSF CAREER Award, as this material is based upon work partially supported by the NSF under CHE-1431172 (Formerly CHE-1151832). AAH would also like to thank Old Dominion University’s Faculty Proposal Preparation Program (FP3) and also the Old Dominion University start-up package that allowed for the successful generation of the tested compounds. SF and TL would like to thank the NSF for their support through the REU Site: Training Undergraduates in Electrochemical Technologies for Clean Fuels (Biofuels and Hydrogen) Production and Applications at Old Dominion University (EEC-1560194). Research reported in this publication was supported by the National Institute of General Medical Sciences of the National Institutes of Health under Award Number T34GM118259. The content is solely the responsibility of the authors and does not necessarily represent the official views of the National Institutes of Health. Matching funds from Old Dominion University is also acknowledged.

This research was also supported in part by an appointment to the Student Research Participation Program at the U.S. Army Engineer Research and Development Center, Construction Engineering Research Laboratory (ERDC-CERL), administered by the Oak Ridge Institute for Science and Education through an interagency agreement between the U.S. Department of Energy and ERDC-CERL.

Abbreviations

$\Delta\Psi_m$
mitochondrial membrane potential

acetylethTSC
(*E*)-*N*-ethyl-2-[1-(thiazol-2-yl)ethylidene]hydrazinecarbothioamide

amtp
3-amino-1,2,4-triazino[5,6-*f*]1,10-phenanthroline

ATCC
American Type Culture Collection

ATS
diacetyl bis(thiosemicarbazone)

ATSC
9-anthraldehydethiosemicarbazone

Bpy
2,2′-bipyridine

BnA
benzylamine

$C_8H_4O_4 2^-$
terephthalate anion

caspase 3
cysteine-aspartic proteases3

ctDNA
calf thymus DNA

DMEM
Dulbecco's Modified Eagle's Medium

dmgBF$_2$
difluoroboryldimethylglyoximato

dpta
dipyrido-[3,2-a;2′,3′-*c*]-thien-[3,4-c]azine

dppz
dipyrido[3,2-a:2′,3′-*c*]-phenazine

EB
ethidium bromide

***N*-ethhymethohcarbthio**
(*E*)-*N*-ethyl-2-(4-hydroxy-3-ethoxybenzylidene)hydrazine-carbothioamide

FBS
fetal bovine serum

FcOHTaman

organometallic ferrocene derivative of hydroxytamoxifen

fmp
2-(4-formylphenyl)imidazo[4,5-*f*][1,10]phenanthroline

fmp-2Br
2-(2′,3-dibromo-4-formyl-phenyl)imidazo[4,5-*f*][1,10]-phenanthroline

GSH
reduced glutathione

GTS
glyoxal bis(thiosemicarbazone)

H4L
1,8-bis(2-hydroxybenzamido)-3,6-diazaoctane

HL^1
2-acetylpyridine-thiosemicarbazone

HL^2
2-acetylpyridine-4-methyl-thiosemicarbazone

HL^3
2-acetylpyridine-4-phenyl-thiosemicarbazone

HMQTS
(*E*)-*N*-methyl-2-(quinolin-2-ylmethylene)hydrazinecarbothioamide

HPQTS
(*E*)-*N*-phenyl-2-(quinolin-2-ylmethylene)hydrazinecarbothioamide

HNAIP
2-(2-hydroxy-l-naphthyl)imidazo[4,5-*f*][1,10]phenanthroline

HRMS
high resolution mass spectra

HSV1
herpes simplex virus 1

hTOP1
human topoisomerase I

hTOP2α
human topoisomerase IIα

hqdppz
5,18-dihydroxynaphtho[2,3-*a*]-dipyrido[3,2-*h*:2′,3′-*f*]phenazine

Im
imidazole

ippip
4-(isopropylbenzaldehyde)imidazo[4,5-*f*][1,10]phenanthroline

L
4-aminobenzenesulphonate

L-pyr
(4-pyridine)oxazolo[4,5-*f*]phenanthroline

MeATSC
9-anthraldehyde-N(4)-methylthiosemicarbazone

MMP
mitochondrial membrane permeabilization

MTS
3-(4,5-dimethylthiazol-2-yl)-5-(3-carboxymethoxyphenyl)-2-(4-sulfophenyl)-2H-tetrazolium

NEAA
non-essential amino acids

OMM
outer mitochondrial membrane

pbt
2-(2′-pyridyl)benzothiazole

pdta
3-(pyridine-2-yl)-as-triazino[5,6-*f*]acenaphthylene

pdtb
3-(pyridine-2-yl)-5,6-diphenyl-as-triazine

pdtp
3-(pyridine-2-yl)-as-triazino[5,6-*f*]phenanthroline

phen
1,10-phenanthroline

PIP
2-phenylimidazo[4,5-*f*][1,10]phenanthroline

pmap
bis(2-(2-pyridyl)ethyl)(2-pyridylmethyl)amine

pmea

bis((2-pyridyl)methyl)-2-((2-pyridyl)ethyl)amine

PTS
pyruvaldehyde bis(thiosemicarbazone)

pyip
2-(1-pyrenyl)-1H-imidazo[4,5-f][phen]

qdppz
naphtho[2,3-*a*]dipyrido[3,2-*h*:2′,3′-*f*]phenazine-5,18-dione

RCD
regulated cell death

sal-*L*-tryp
N-salicylidene-*L*-tryptophanate

SDS
sodium dodecyl sulfate

Tepa
tris(2-(2-pyridyl)ethyl)amine

TMRE
tetramethylrhodamine, ethyl ester

TNBC
triple-negative breast cancer

Tpa
tris(2-pyridylmethyl)amine

Tpphz
tetrapyrido-[3,2-*a*:2′,3′-*c*:3″,2″-h:2‴,3‴-j]phenazine

References

[1]. Acevedo-Diaz A, Ortiz-Soto G, Suarez-Arroyo IJ, Martinez MMM, Zayas-Santiago A, Nutrients, vol. (2019) 11.

[2]. Misra A, Ahmad R, Trivedi A, Khan MA, J. Basic Clin Pharm., vol. 8, Global Scientific Research Forum (2017) S72–S79.

[3]. Roberson PNE, Miller M, Lloyd J, Bell C, Eric HR, J. Bell, Cancer Treat, Res. Commun. 19 (2019) 100128.

[4]. Wani K, Tarawadi K, Kaul-Ghanekar R, J. Nano Res. 34 (2015) 29–40.

[5]. Yedjou CG, Tchounwou PB, Payton M, Miele L, Fonseca DD, Lowe L, Alo RA, Int. J. Environ. Res. Public Health, vol. 14, 2017, pp. 14050486/14050481–14050486/14050414.

[6]. Alexopoulou AN, Ho-Yen CM, Papalazarou V, Elia G, Jones JL, Hodivala-Dilke K, BMC Cancer 14 (2014) 237/231–237/238.

[7]. Kulkarni S, Augoff K, Rivera L, McCue B, Khoury T, Groman A, Zhang L, Tian L, Sossey-Alaoui K, PLoS One 7 (2012) e42895.

[8]. Tot T, Cancer 110 (2007) 2551–2560. [PubMed: 17932896]

[9]. Ma H, Ursin G, Xu X, Lee E, Togawa K, Duan L, Lu Y, Malone KE, Marchbanks PA, McDonald JA, Simon MS, Folger SG, Sullivan-Halley J, Deapen DM, Press MF, Bernstein L, Breast Cancer Res. 19 (2017) 6. [PubMed: 28086982]

[10]. Anders CK, Johnson R, Litton J, Phillips M, Bleyer A, Semin. Oncol 36 (2009) 237–249. [PubMed: 19460581]

[11]. Dietze EC, Sistrunk C, Miranda-Carboni G, O'Regan R, Seewaldt VL, Nat. Rev. Cancer 15 (2015) 248–254. [PubMed: 25673085]

[12]. Cardoso F, Harbeck N, Fallowfield L, Kyriakides S, Senkus E, Ann. Oncol 23 (2012) 19. [PubMed: 21508174]

[13]. Weigelt B, Peterse JL, van't Veer LJ, Nat. Rev. Cancer 5 (2005) 591–602. [PubMed: 16056258]

[14]. Weide R, Feiten S, Friesenhahn V, Heymanns J, Kleboth K, Thomalla J, van Roye C, Köppler H, SpringerPlus 3 (2014) 535. [PubMed: 25279326]

[15]. Stockler M, Wilcken NRC, Ghersi D, Simes RJ, Cancer Treat, Rev. 26 (2000) 151–168. [PubMed: 10814559]

[16]. Giuliani J, Bonetti A, Tumori J. 101 (2015) 347–352.

[17]. Eng LG, Dawood S, Dent R, Curr. Opin. Support Palliat. Care 9 (2015) 301–307. [PubMed: 26155021]

[18]. Lewis S, Yee J, Kilbreath S, Willis K, Breast 24 (2015) 242–247. [PubMed: 25753212]

[19]. Wheatley-Price P, Ali M, Balchin K, Spencer J, Fitzgibbon E, Cripps C, Curr. Oncol 21 (2014) 187–192. [PubMed: 25089101]

[20]. Wong E, Giandomenico CM, Chem. Rev 99 (1999) 2451–2466. [PubMed: 11749486]

[21]. Galanski M, Arion VB, Jakupec MA, Keppler BK, Curr. Pharm. Des 9 (2003) 2078–2089. [PubMed: 14529417]

[22]. Jakupec MA, Galanski M, Keppler BK, Rev. Physiol., Biochem. Pharm 146 (2003) 1–54.

[23]. Ott I, Gust R, Arch. Pharm 340 (2007) 117–126.

[24]. Bratsos I, Jedner S, Gianferrara T, Alessio E, Chimia 61 (2007) 692–697.

[25]. Hartinger CG, Jakupec MA, Zorbas-Seifried S, Groessl M, Egger A, Berger W, Zorbas H, Dyson PJ, Keppler BK, Chem. Biodivers 5 (2008) 2140–2155. [PubMed: 18972504]

[26]. Jakupec MA, Galanski M, Arion VB, Hartinger CG, Keppler BK, Dalton Trans, 2008, pp. 183–194. [PubMed: 18097483]

[27]. Ott I, Coord. Chem. Rev 253 (2009) 1670–1681.

[28]. Bergamo A, Sava G, Dalton Trans, vol. 40, T (2011) 7817–7823. [PubMed: 21629963]

[29]. Kostova I, Anti-Cancer Agents Med, Chem. 9 (2009) 827–842.

[30]. Bergamo A, Gaiddon C, Schellens JHM, Beijnen JH, Sava G, J. Inorg. Biochem 106 (2012) 90–99. [PubMed: 22112845]

[31]. Chitambar CR, Future Med, Chem. 4 (2012) 1257–1272. [PubMed: 22800370]

[32]. Hall MD, Failes TW, Yamamoto N, Hambley TW, Dalton Trans, 2007, pp. 3983–3990. [PubMed: 17828357]

[33]. Cazares-Marinero J.d.J., Top S, Vessieres A, Jaouen G, Dalton Trans. 43 (2014) 817–830. [PubMed: 24153445]

[34]. Cazares Marinero J.d.J., Lapierre M, Cavailles V, Saint-Fort R, Vessieres A, Top S, Jaouen G, Dalton Trans. 42 (2013) 15489–15501. [PubMed: 24030275]

[35]. Laine A-L, Adriaenssens E, Vessieres A, Jaouen G, Corbet C, Desruelles E, Pigeon P, Toillon R-A, Passirani C, Biomaterials 34 (2013) 6949–6956. [PubMed: 23777919]

[36]. Davila-Rodriguez M-J, Barolli JP, de Oliveira KM, Colina-Vegas L, da Silva Miranda F, Castellano EE, Von Poelhsitz G, Batista AA, Arch. Biochem. Biophys 660 (2018) 156–167. [PubMed: 30389443]

[37]. Havrylyuk D, Deshpande M, Parkin S, Glazer EC, Chem. Commun 54 (2018) 12487–12490.

[38]. Kumar A, Dixit A, Banerjee S, Mukherjee S, Sahoo S, Karande AA, Chakravarty AR, Indian J, Chem., Sect. A: Inorg., Bio-inorg., Phys., Theor. Anal, Chem 57A (2018) 409–417.

[39]. Liu B, Monro S, Lystrom L, Cameron CG, Colon K, Yin H, Kilina S, McFarland SA, Sun W, Inorg. Chem 57 (2018) 9859–9872. [PubMed: 30091916]

[40]. Ma G-L, Bi X-D, Gao F, Feng Z, Zhao D-C, Lin F-J, Yan R, Liu D, Liu P, Chen J, Zhang H, J. Inorg. Biochem 185 (2018) 1–9. [PubMed: 29730231]

[41]. Zhang P, Huang H, Dalton Trans. 47 (2018) 14841–14854. [PubMed: 30325378]

[42]. Holder AA, Zigler DF, Tarrago-Trani MT, Storrie B, Brewer KJ, Inorg. Chem 46 (2007) 4760. [PubMed: 17488069]

[43]. Storrie B, Holder A, Brewer KJ, Proc. SPIE-The International Society for Optical Engineering 6139 (2006) 336–342.

[44]. Swavey S, Fang Z, Brewer KJ, Inorg. Chem 41 (2002) 2598–2607. [PubMed: 11978132]

[45]. Williams RL, Toft HN, Winkel B, Brewer KJ, Inorg. Chem 42 (2003) 4394–4400. [PubMed: 12844312]

[46]. Barton JK, Danishefsky A, Goldberg J, J. Am. Chem. Soc 106 (1984) 2172–2176.

[47]. Holder AA, Swavey S, Brewer KJ, Inorg. Chem 43 (2004) 303. [PubMed: 14704081]

[48]. Holder AA, Taylor P, Magnusen AR, Moffett ET, Meyer K, Hong Y, Ramsdale SE, Gordon M, Stubbs J, Seymour LA, Acharya D, Weber RT, Smith PF, Dismukes GC, Ji P, Menocal L, Bai F, Williams JL, Cropek DM, Jarrett WL, Dalton Trans. 42 (2013) 11881–11899. [PubMed: 23783642]

[49]. Craver E, McCrate A, Nielsen M, Swavey S, Inorg. Chim. Acta 363 (2010) 453–456.

[50]. Du K-J, Wang J-Q, Kou J-F, Li G-Y, Wang L-L, Chao H, Ji L-N, Eur. J. Med. Chem 46 (2011) 1056–1065. [PubMed: 21295892]

[51]. Gao F, Chao H, Zhou F, Chen X, Wei Y-F, Ji L-N, J. Inorg. Biochem 102 (2008) 1050–1059. [PubMed: 18295337]

[52]. Huang H-L, Li Z-Z, Liang Z-H, Liu Y-J, Eur. J. Inorg. Chem 2011 (2011) 5538–5547.

[53]. Lawrence Arockiasamy D, Radhika S, Parthasarathi R, Nair BU, Eur. J. Med. Chem 44 (2009) 2044–2051. [PubMed: 19026470]

[54]. Liu X-W, Xu L-C, Li H, Chao H, Zheng K-C, Ji L-N, J. Mol. Struct 920 (2009) 163–171.

[55]. McCrate A, Carlone M, Nielsen M, Swavey S, Inorg. Chem. Commun 13 (2010) 537–539.

[56]. Moody L, Holder AA, Annu. Rep. Prog. Chem., Sect. A: Inorg, Chem. 105 (2009) 505–524.

[57]. O'Reilly F, Kelly J, A, Chem. Commun, Kirsch-De Mesmaeker, 1996, pp. 1013–1014.

[58]. Reddy KL, Reddy YHK, Satyanarayana S, Nucleos. Nucleot. Nucl 28 (2009) 953–968.

[59]. Sun S, He Y, Yang Z, Pang Y, Liu F, Fan J, Sun L, Peng X, Dalton Trans. 39 (2010) 4411–4416. [PubMed: 20422098]

[60]. Miao T-F, Li J, Liao S-Y, Mei J, Zheng K-C, THEOCHEM J. Mol. Struct 957 (2010) 108–113.

[61]. Naik HRP, Naik HSB, Lamani DS, Aravinda T, Kumar BV, Kumar BV, Yogesh M, Sharath N, Kumar PNP, Macromol J, Sci., Part A: Pure Appl, Chem. 46 (2009) 790–795.

[62]. Naik HSB, Prabhakara MC, BioChem.: Indian Journal 1 (2007) 126–132.

[63]. Peng B, Chao H, Sun B, Li H, Gao F, Ji L-N, J. Inorg. Biochem 101 (2007) 404–411. [PubMed: 17196659]

[64]. Prabahkara MC, Bhojya Naik HS, BioMetals 21 (2008) 675–684. [PubMed: 18581241]

[65]. Roy S, Saha S, Majumdar R, Dighe RR, Chakravarty AR, Inorg. Chem 48 (2009) 9501–9509. [PubMed: 19719144]

[66]. Balaji B, Perumalla S, Balakrishnan B, Karande AA, Chakravarty AR, Eur. J. Med. Chem 85 (2014) 458–467. [PubMed: 25113874]

[67]. Balaji B, Somyajit K, Banik B, Nagaraju G, Chakravarty AR, Inorg. Chim. Acta 400 (2013) 142–150.

[68]. Banerjee S, Hussain A, Prasad P, Khan I, Banik B, Kondaiah P, Chakravarty AR, Eur. J. Inorg. Chem 2012 (2012) 3899–3908 (S3899/3891-S3899/3811).

[69]. Banerjee S, Pant I, Khan I, Prasad P, Hussain A, Kondaiah P, Chakravarty AR, Dalton Trans. 44 (2015) 4108–4122. [PubMed: 25623080]

[70]. Banik B, Somyajit K, Koley D, Nagaraju G, Chakravarty AR, Inorg. Chim. Acta 393 (2012) 284–293.

[71]. Bhattacharyya U, Kumar B, Garai A, Bhattacharyya A, Kumar A, Banerjee S, Kondaiah P, Chakravarty AR, Inorg. Chem 56 (2017) 12457–12468. [PubMed: 28972748]

[72]. Chen C-T, Lin J-S, Kuo J-H, Weng S-S, Cuo T-S, Lin Y-W, Cheng C-C, Huang Y-C, Yu J-K, Chou P-T, Org. Lett 6 (2004) 4471–4474. [PubMed: 15548053]

[73]. Chou P-T, Lee M-Z, Wei C-Y, Wu G-R, Shek LK, Kwong DWJ, Photochem. Photobiol 70 (1999) 745–750.

[74]. Du Y.-f., Lu J-Z, Guo H.-w., Jiang J, Chao P, Chen F, Pan J-M, Transition Met, Chem. 35 (2010) 859–864.

[75]. Guo H, Lu J, Ruan Z, Zhang Y, Liu Y, Zang L, Jiang J, Huang J, J. Coord. Chem 65 (2012) 191–204.

[76]. Kwong DWJ, Chan OY, Wong RNS, Musser SM, Vaca L, Chan SI, Inorg. Chem 36 (1997) 1276–1277. [PubMed: 11669701]

[77]. Prasad P, Khan I, Sasmal PK, Koley D, Kondaiah P, Chakravarty AR, Chem. Commun 47 (2011) 3954–3956.

[78]. Prasad P, Pant I, Khan I, Kondaiah P, Chakravarty AR, Eur. J. Inorg. Chem 2014 (2014) 2420–2431.

[79]. Sasmal PK, Saha S, Majumdar R, Dighe RR, Chakravarty AR, Inorg. Chem 49 (2010) 849–859. [PubMed: 20039725]

[80]. Sasmal PK, Saha S, Majumdar R, Dighe RR, A.R, Chem. Commun, Chakravarty, 2009, pp. 1703–1705.

[81]. Schwartz JA, Lium EK, Silverstein SJ, Virol J. 75 (2001) 4117–4128.

[82]. Chang EL, Simmers C, Knight DA, Pharmaceuticals 3 (2010) 1711. [PubMed: 27713325]

[83]. Munteanu CR, Suntharalingam K, Dalton Trans. 44 (2015) 13796–13808. [PubMed: 26148776]

[84]. Chylewska A, Biedulska M, Sumczynski P, Makowski M, Curr. Med. Chem 25 (2018) 1729–1791. [PubMed: 29210637]

[85]. Cressey PB, Eskandari A, Bruno PM, Lu C, Hemann MT, Suntharalingam K, ChemBioChem 17 (2016) 1713–1718. [PubMed: 27377813]

[86]. Cressey PB, Eskandari A, Suntharalingam K, Inorganics 5 (2017) 12/11–12/13.

[87]. King AP, Gellineau HA, Ahn J-E, MacMillan SN, Wilson JJ, Inorg. Chem 56 (2017) 6609–6623. [PubMed: 28509538]

[88]. Renfrew AK, O'Neill ES, Hambley TW, New EJ, Coord. Chem. Rev 375 (2018) 221–233.

[89]. Zhang P, Sadler PJ, Eur. J. Inorg. Chem 2017 (2017) 1541–1548.

[90]. Arounaguiri S, Easwaramoorthy D, Ashokkumar A, Dattagupta A, Maiya BG, Proc. - Indian Acad. Sci, Chem. Sci 112 (2000) 1–17.

[91]. Barton JK, Paranawithana SR, Biochemistry 25 (1986) 2205–2211. [PubMed: 3011080]

[92]. Katner SJ, Johnson WE, Peterson EJ, Page P, Farrell NP, Inorg. Chem 57 (2018) 3116–3125. [PubMed: 29473748]

[93]. Proudfoot EM, Mackay JP, Karuso P, Biochemistry 40 (2001) 4867–4878. [PubMed: 11294655]

[94]. Sastri CV, Mariappan M, Ghosh T, Maiya BG, Proc. Indian Natl. Sci. Acad, Part A 70 (2004) 355–365.

[95]. Barton JK, Science 233 (1986) 727–734. [PubMed: 3016894]

[96]. Carter MT, Rodriguez M, Bard AJ, J. Am. Chem. Soc 111 (1989) 8901–8911.

[97]. Soenmez M, Celebi M, Yardim Y, Sentuerk Z, Eur. J. Med. Chem 45 (2010) 4215–4220. [PubMed: 20619510]

[98]. Vijayalakshmi R, Kanthimathi M, Subramanian V, Nair BU, Biochim. Biophys. Acta, Gen, Subj. 1475 (2000) 157–162.

[99]. Aslanoglu M, Horrocks BR, Proc. - Electrochem, Soc. 97–19 (1997) 345–356.

[100]. Aslanoglu M, Isaac CJ, Houlton A, Horrocks BR, Analyst 125 (2000) 1791–1798. [PubMed: 11070548]

[101]. Del Pozo MV, Alonso C, Pariente F, Lorenzo E, Biosens. Bioelectron 20 (2005) 1549–1558. [PubMed: 15626608]

[102]. Erdem A, Meric B, Kerman K, Dalbasti T, Ozsoz M, Electroanalysis 11 (1999) 1372–1376.

[103]. Keypour H, Forouzandeh F, Salehzadeh S, Hajibabaei F, Feizi S, Karamian R, Ghiasi N, Gable RW, Polyhedron 170 (2019) 584–592.

[104]. Shahabadi N, Moradi Fili S, J. Coord. Chem 71 (2018) 2843–2855.

[105]. Barton JK, Comments Inorg, Chem. 3 (1985) 321–348.

[106]. Murali S, Sastri CV, Maiya BG, Proc. - Indian Acad. Sci, Chem. Sci. 114 (2002) 403–415.

[107]. Raman N, Arun TR, Mahalakshmi R, Packianathan S, Antony R, Inorg. Chem. Commun 46 (2014) 263–267.

[108]. Raman N, Mahalakshmi R, Arun T, Packianathan S, Rajkumar R, J. Photochem, Photobiol, B 138 (2014) 211–222. [PubMed: 24976625]

[109]. Raman N, Selvaganapathy M, Radhakrishnan S, Spectrochim, Acta, Part A 127 (2014) 185–195.

[110]. Hall MD, Salam NK, Hellawell JL, Fales HM, Kensler CB, Ludwig JA, Szakacs G, Hibbs DE, Gottesman MM, J. Med. Chem 52 (2009) 3191–3204. [PubMed: 19397322]

[111]. Jansson PJ, Sharpe PC, Bernhardt PV, Richardson DR, J. Med. Chem 53 (2010) 5759–5769. [PubMed: 20597487]

[112]. Easmon J, Puerstinger G, Heinisch G, Roth T, Fiebig HH, Holzer W, Jaeger W, Jenny M, Hofmann J, J. Med. Chem 44 (2001) 2164–2171. [PubMed: 11405653]

[113]. Saryan LA, Ankel E, Krishnamurti C, Petering DH, Elford H, J. Med. Chem 22 (1979) 1218–1221. [PubMed: 513069]

[114]. Kowol CR, Berger R, Eichinger R, Roller A, Jakupec MA, Schmidt PP, Arion VB, Keppler BK, J. Med. Chem 50 (2007) 1254–1265. [PubMed: 17315858]

[115]. Matesanz AI, Souza P, Mini-Rev. Med. Chem 9 (2009) 1389–1396. [PubMed: 19929812]

[116]. Zeglis BM, Divilov V, Lewis JS, J. Med. Chem 54 (2011) 2391–2398. [PubMed: 21391686]

[117]. Yu Y, Kalinowski DS, Kovacevic Z, Siafakas AR, Jansson PJ, Stefani C, Lovejoy DB, Sharpe PC, Bernhardt PV, Richardson DR, J. Med. Chem 52 (2009) 5271–5294. [PubMed: 19601577]

[118]. Tarasconi P, Capacchi S, Pelosi G, Cornia M, Albertini R, Bonati A, Dall'Aglio PP, Lunghi P, Pinelli S, Bioorg. Med. Chem 8 (2000) 157–162. [PubMed: 10968274]

[119]. West DX, Swearingen JK, Valdes-Martinez J, Hernandez-Ortega S, El-Sawaf AK, Van Meurs F, Castineiras A, Garcia I, Bermejo E, Polyhedron 18 (1999) 2919–2929.

[120]. Milunovic MNM, Enyedy ÉA, Nagy NV, Kiss T, Trondl R, Jakupec MA, Keppler BK, Krachler R, Novitchi G, Arion VB, Inorg. Chem 51 (2012) 9309–9321. [PubMed: 22889304]

[121]. Renfrew AK, Metallomics 6 (2014) 1324–1335. [PubMed: 24850462]

[122]. Rautio J, Kumpulainen H, Heimbach T, Oliyai R, Oh D, Järvinen T, Savolainen J, Nat. Rev. Drug Discov 7 (2008) 255–270. [PubMed: 18219308]

[123]. Johnson TJ, Hedge DD, Am. J. Health-Syst. Pharm 59 (2002) 1333–1339. [PubMed: 12132559]

[124]. Demoro B, Caruso F, Rossi M, Benitez D, Gonzalez M, Cerecetto H, Parajon-Costa B, Castiglioni J, Galizzi M, Docampo R, Otero L, Gambino D, J. Inorg. Biochem 104 (2010) 1252–1258. [PubMed: 20817265]

[125]. Puckett CA, Ernst RJ, Barton JK, Dalton Trans. 39 (2010) 1159–1170. [PubMed: 20104335]

[126]. Qu F, Park S, Martinez K, Gray JL, Thowfeik FS, Lundeen JA, Kuhn AE, Charboneau DJ, Gerlach DL, Lockart MM, Law JA, Jernigan KL, Chambers N, Zeller M, Piro NA, Kassel WS, Schmehl RH, Paul JJ, Merino EJ, Kim Y, Papish ET, Inorg. Chem 56 (2017) 7519–7532. [PubMed: 28636344]

[127]. Graf N, Lippard SJ, Adv. Drug Deliv. Rev 64 (2012) 993–1004. [PubMed: 22289471]

[128]. Pothig A, Casini A, Casini A, Theranostics 9 (2019) 3150–3169. [PubMed: 31244947]

[129]. Zhang D, Wu M, Cai Z, Liao N, Ke K, Liu H, Li M, Liu G, Yang H, Liu X, Liu J, Adv. Sci, vol. 5, 2018, pp. 1700648.

[130]. Weder JE, Dillon CT, Hambley TW, Kennedy BJ, Lay PA, Biffin JR, Regtop HL, Davies NM, Coord. Chem. Rev 232 (2002) 95–126.

[131]. Fedorowicz J, Sączewski J, Monatsh. Chem 149 (2018) 1199–1245. [PubMed: 29983452]

[132]. Jagadeesan S, Balasubramanian V, Baumann P, Neuburger M, Häussinger D, Palivan CG, Inorg. Chem 52 (2013) 12535–12544. [PubMed: 24127683]

[133]. Ramachandran E, Thomas SP, Poornima P, Kalaivani P, Prabhakaran R, Padma VV, Natarajan K, Eur. J. Med. Chem 50 (2012) 405–415. [PubMed: 22397923]

[134]. Bisceglie F, Tavone M, Mussi F, Azzoni S, Montalbano S, Franzoni S, Tarasconi P, Buschini A, Pelosi G, J. Inorg. Biochem 179 (2018) 60–70. [PubMed: 29175629]

[135]. Hall IH, Miller MC, West DX III, Met.-Based Drugs 4 (1997) 89–95. [PubMed: 18475774]

[136]. Todorovic TR, Vukasinovic J, Portalone G, Suleiman S, Gligorijevic N, Bjelogrlic S, Jovanovic K, Radulovic S, Andjelkovic K, Cassar A, Filipovic NR, Schembri-Wismayer P, MedChemComm 8 (2017) 103–111. [PubMed: 30108695]

[137]. Kerr JF, Wyllie AH, Currie AR, Br. J. Cancer 26 (1972) 239–257. [PubMed: 4561027]

[138]. Radogna F, Dicato M, Diederich M, Biochem. Pharmacol 94 (2015) 1–11. [PubMed: 25562745]

[139]. Galluzzi L, Vitale I, Abrams JM, Alnemri ES, Baehrecke EH, Blagosklonny MV, Dawson TM, Dawson VL, El-Deiry WS, Fulda S, Gottlieb E, Green DR, Hengartner MO, Kepp O, Knight RA, Kumar S, Lipton SA, Lu X, Madeo F, Malorni W, Mehlen P, Nunez G, Peter ME, Piacentini M, Rubinsztein DC, Shi Y, Simon HU, Vandenabeele P, White E, Yuan J, Zhivotovsky B, Melino G, Kroemer G, Cell Death Differ. 19 (2012) 107–120. [PubMed: 21760595]

[140]. Beckford FA, Shaloski M Jr., Leblanc G, Thessing J, Lewis-Alleyne LC, Holder AA, Li L, Seeram NP, Dalton Trans, 2009, pp. 10757–10764. [PubMed: 20023905]

[141]. Tao S, Xu S, Zhang X, Chem. Phys. Lett 429 (2006) 622–627.

[142]. Kim HN, Lim J, Lee HN, Ryu J-W, Kim MJ, Lee J, Lee D-U, Kim Y, Kim S-J, Lee KD, Lee H-S, Yoon J, Org. Lett 13 (2011) 1314–1317. [PubMed: 21348457]

[143]. Wunz TP, Dorr RT, Alberts DS, Tunget CL, Einspahr J, Milton S, Remers WA, J. Med. Chem 30 (1987) 1313–1321. [PubMed: 2441053]

[144]. Pittillo RF, Woolley C, Appl. Microbiol 18 (1969) 519–521. [PubMed: 5373683]

[145]. Modukuru NK, Snow KJ, Perrin BS Jr., Thota J, Kumar CV, J. Phys. Chem. B 109 (2005) 11810–11818. [PubMed: 16852450]

[146]. Wunz TP, Craven MT, Karol MD, Hill GC, Remers WA, J. Med. Chem 33 (1990) 1549–1553. [PubMed: 2342051]

[147]. Iyengar BS, Dorr RT, Alberts DS, Solyom AM, Krutzsch M, Remers WA, J. Med. Chem 40 (1997) 3734–3738. [PubMed: 9371238]

[148]. Dorr RT, Liddil JD, Sami SM, Remers W, Hersh EM, Alberts DS, Anti-Cancer Drugs 12 (2001) 213–220. [PubMed: 11290869]

[149]. Tao K, Fang M, Alroy J, Sahagian GG, BMC Cancer 8 (2008) 228. [PubMed: 18691423]

[150]. Heppner GH, Miller FR, Shekhar PM, Breast Cancer Res. 2 (2000) 331–334. [PubMed: 11250725]

[151]. Bailey-Downs LC, Thorpe JE, Disch BC, Bastian A, Hauser PJ, Farasyn T, Berry WL, Hurst RE, Ihnat MA, PLoS One 9 (2014) e98624.

[152]. Taura T, Bull. Chem. Soc. Jpn 63 (1990) 1105–1110.

[153]. Kashiwabara K, Igi K, Douglas BE, Bull. Chem. Soc. Jpn 49 (1976) 1573–1578.

[154]. Sharma RP, Singh A, Venugopalan P, Harrison WTA, J. Mol. Struct 980 (2010) 72–77.

[155]. Ye B-H, Chen X-M, Zeng T-X, Ji LN, Polyhedron 13 (1994) 2185–2191.

[156]. van Wieren-de Wijer DB, Maitland-van der Zee AH, de Boer A, Belitser SV, Kroon AA, de Leeuw PW, Schiffers P, Janssen RG, van Duijn CM, Stricker BH, Klungel OH, Eur. J. Epidemiol 24 (2009) 677–682. [PubMed: 19760105]

[157]. Zhu CX, Tse-Dinh YC, J. Biol. Chem 275 (2000) 5318–5322. [PubMed: 10681504]

[158]. Bansal S, Sinha D, Singh M, Cheng B, Tse-Dinh YC, Tandon V, J. Antimicrob. Chemother 67 (2012) 2882–2891. [PubMed: 22945915]

[159]. Beebe SJ, Sain NM, Ren W, Cells, vol. 2, MDPI (2013) 136–162. [PubMed: 24709649]

[160]. Wu S, Guo J, Wei W, Zhang J, Fang J, Beebe SJ, Cancer Cell Int, vol. 14, 2014, pp. 98/91–98/12.

[161]. Lewis NA, Liu F, Seymour L, Magnusen A, Erves TR, Arca JF, Beckford FA, Venkatraman R, González-Sarrías A, Fronczek FR, VanDerveer DG, Seeram NP, Liu A, Jarrett WL, Holder AA, Eur. J. Inorg. Chem 2012 (2012) 664–677. [PubMed: 23904789]

[162]. Kate AN, Kumbhar AA, Khan AA, Joshi PV, Puranik VG, Bioconjug. Chem 25 (2014) 102–114. [PubMed: 24328322]

[163]. Sobiesiak M, Cieslak M, Krolewska K, Kazmierczak-Baranska J, Pasternak B, Budzisz E, J. New, Chem 40 (2016) 9761–9767.

[164]. Xiong H, Motchelaho MAM, Moyo M, Jewell LL, Coville NJ, Catal J. 278 (2011) 26–40.

[165]. Xiong H, Moyo M, Rayner MK, Jewell LL, Billing DG, Coville NJ, ChemCatChem 2 (2010) 514–518.

[166]. Yang Y, Jia L, Hou B, Li D, Wang J, Sun Y, Catal. Sci. Technol 4 (2014) 717–728.

[167]. Yang Y, Jia L, Hou B, Li D, Wang J, Sun Y, ChemCatChem 6 (2014) 319–327

[168]. Vondrova M, McQueen TM, Burgess CM, Ho DM, Bocarsly AB, J. Am. Chem. Soc 130 (2008) 5563–5572. [PubMed: 18366164]

[169]. Kitagawa S, Munakata M, Higashie A, Inorg. Chim. Acta 84 (1984) 79–84.

[170]. Popova M, Ristic A, Mazaj M, Maucec D, Dimitrov M, Tusar NN, ChemCatChem 6 (2014) 271–277.

[171]. Sushkevich VL, Smirnov AV, van Bokhoven JA, Phys J, Chem. C 123 (2019) 9926–9934.

[172]. Turnbull MM, Pon G, Willett RD, Polyhedron 10 (1991) 1835–1838.

[173]. Sutradhar M, Roy Barman T, Klanke J, Drew MGB, Rentschler E, Polyhedron 53 (2013) 48–55.

[174]. Jardine FH, in: Emeléus HJ, Sharpe AG (Eds.), Advances in Inorganic Chemistry and Radiochemistry, vol. 17, Academic Press, 1975, pp. 115–163.

[175]. Fedorova OA, Shepel NE, Tokarev SD, Lukovskaya EV, Sotnikova YA, Moiseeva AA, D'Aléo A, Fages F, Maurel F, Fedorov YV, New J. Chem. 43 (2019) 2817–2827.

[176]. Geary WJ, Coord. Chem. Rev 7 (1971) 81–122.

[177]. Sandhaus S, Taylor R, Edwards T, Huddleston A, Wooten Y, Venkatraman R, Weber RT, González-Sarrías A, Martin P, Cagle P, Tse-Dinh YC, Beebe SJ, Seeram N, Holder AA, Inorg. Chem. Commun 64 (2016) 45–49. [PubMed: 26752972]

[178]. Beckford FA, Thessing J, Stott A, Holder AA, Poluektov OG, Li L, Seeram NP, Inorg. Chem. Commun 15 (2012) 225–229. [PubMed: 23440300]

[179]. Goebbert DJ, Garand E, Wende T, Bergmann R, Meijer G, Asmis KR, Neumark DM, J. Phys. Chem. A 113 (2009) 7584–7592. [PubMed: 19445493]

[180]. Miller FA, Wilkins CH, Anal. Chem 24 (1952) 1253–1294.

[181]. Lobana TS, Sánchez A, Casas JS, Castiñeiras A, Sordo J, García-Tasende MS, Vázquez-López EM, J. Chem. Soc. Dalton Trans (1997) 4289–4300.

[182]. Harness R, Robertson C, Beckford F, J. Undergrad. Chem. Res 7 (2008) 92–97.

[183]. Beckford FA, Stott A, Mbarushimana PC, LeBlanc M-A, Hall K, Smith S, Bullock J, Houghton D, Holder A, Gerasimchuk N, Interdiscip. J. Chem 1 (1) (2016).

[184]. von Philipsborn W, Chem. Soc, Rev 28 (1999) 95–105.

[185]. Barnard I, Koch KR, Inorg. Chim. Acta, vol. 495, 2019, pp. 119019.

[186]. Yamasaki A, J. Coord. Chem 24 (1991) 211–260.

[187]. Harris RK, Chem. Soc. Rev 5 (1976) 1–22.

[188]. Medek A, Frydman V, Frydman L, Proc. Natl. Acad. Sci, USA 94 (1997) 14237–14242. [PubMed: 9405596]

[189]. Cropek DM, Metz A, Muller AM, Gray HB, Horne T, Horton DC, Poluektov O, Tiede DM, Weber RT, Jarrett WL, Phillips JD, Holder AA, Dalton Trans 41 (2012) 13060–13073. [PubMed: 23001132]

[190]. Lawrence MAW, Holder AA, Inorg. Chim. Acta 441 (2016) 157–168.

[191]. Healy PC, Hanna JV, Duffy NV, Skelton BW, White AH, Aust. J. Chem 43 (1990) 1335–1346.

[192]. Hagen KI, Schwab CM, Edwards JO, Jones JG, Lawler RG, Sweigart DA, J. Am. Chem. Soc 110 (1988) 7024–7031.

[193]. Hagen KI, Schwab CM, Edwards JO, Sweigart DA, Inorg. Chem 25 (1986) 978–983.

[194]. Taura T, Bull. Chem. Soc. Jpn 64 (1991) 2362–2371.

[195]. Navon G, Panigel R, Inorg. Chem 28 (1989) 1405–1407.

[196]. Jamieson ER, Lippard SJ, Chem. Rev 99 (1999) 2467–2498. [PubMed: 11749487]

[197]. Singh BK, Asian J, Chem. 17 (2005) 1–32.

[198]. Grabner S, Kosmrlj J, Bukovec N, Cemazar M, J. Inorg. Biochem 95 (2003) 105–112. [PubMed: 12763654]

[199]. Sugden KD, Stearns DM, J. Environ, Pathol, Toxicol. Oncol. 19 (2000) 215–230. [PubMed: 10983888]

[200]. Verma A, Simard JM, Worrall JWE, Rotello VM, J. Am. Chem. Soc 126 (2004) 13987–13991. [PubMed: 15506760]

[201]. Dixon DA, Dasgupta TP, Sadler NP, Inorg. React. Mech 1 (1998) 41–56.

[202]. Nayak S, Reddy KV, Dash AC, Transition Met, Chem. 39 (2014) 177–187.

[203]. Selvi PT, Palaniandavar M, Inorg. Chim. Acta 337 (2002) 420–428.

[204]. Uma V, Castineiras A, Nair BU, Polyhedron 26 (2007) 3008–3016.

[205]. Wolfe A, Shimer GH Jr., Meehan T, Biochemistry 26 (1987) 6392–6396. [PubMed: 3427013]

[206]. Indumathy R, Weyhermüller T, Nair BU, Dalton Trans. 39 (2010) 2087–2097. [PubMed: 20148229]

[207]. Ghosh S, Barve AC, Kumbhar AA, Kumbhar AS, Puranik VG, Datar PA, Sonawane UB, Joshi RR, J. Inorg. Biochem. 100 (2006) 331–343. [PubMed: 16412513]

[208]. Aleo D, Cardile V, Chillemi R, Granata G, Sciuto S, Nat. Prod. Commun, vol. 3, 2008, pp. 1934578X0800301023.

[209]. Janjua NK, Siddiqa A, Yaqub A, Sabahat S, Qureshi R, Haque S.u., Spectrochim, Acta Part A 74 (2009) 1135–1137.

[210]. Zegar IS, Prakash AS, Harvey RG, LeBreton PR, J. Am. Chem. Soc 107 (1985) 7990–7995.

[211]. Wang X-L, Chao H, Li H, Hong X-L, Liu Y-J, Tan L-F, Ji L-N, J. Inorg. Biochem 98 (2004) 1143–1150. [PubMed: 15149826]

[212]. LePecq JB, Paoletti C, J. Mol. Biol 27 (1967) 87–106. [PubMed: 6033613]

[213]. Friedman AE, Chambron JC, Sauvage JP, Turro NJ, Barton JK, J. Am. Chem. Soc 112 (1990) 4960–4962.

[214]. Erkkila KE, Odom DT, Barton JK, Chem. Rev 99 (1999) 2777–2795. [PubMed: 11749500]

[215]. Haworth IS, Elcock AH, Freeman J, Rodger A, Richards WG, J. Biomol. Struct. Dyn 9 (1991) 23–44. [PubMed: 1781946]

[216]. Kelly JM, Tossi AB, McConnell DJ, OhUigin C, Nucleic Acids Res. 13 (1985) 6017–6034. [PubMed: 4047939]

[217]. Tysoe SA, Morgan RJ, Baker AD, Strekas TC, J. Phys. Chem 97 (1993) 1707–1711.

[218]. Beckford FA, Niece MB, Lassiter BP, Beebe SJ, Holder AA, J. Biol. Inorg. Chem 23 (2018) 1205–1217. [PubMed: 30039184]

[219]. Lutterman DA, Chouai A, Liu Y, Sun Y, Stewart CD, Dunbar KR, Turro C, J. Am. Chem. Soc 130 (2008) 1163–1170. [PubMed: 18179207]

[220]. Baguley BC, Le Bret M, Biochemistry 23 (1984) 937–943. [PubMed: 6546881]

[221]. Maartensson AKF, Lincoln P, Phys. Chem. Chem. Phys 20 (2018) 7920–7930. [PubMed: 29308462]

[222]. Demarse NA, Killian MC, Hansen LD, Quinn CF, Methods Mol. Biol (New York, NY, United States), vol. 978, Springer, 2013, pp. 21–30. [PubMed: 23423886]

[223]. Drozdz W, Walczak A, Bessin Y, Gervais V, Cao X-Y, Lehn J-M, Ulrich S, Stefankiewicz AR, Chem. Eur. J 24 (2018) 10802–10811. [PubMed: 29741793]

[224]. Khan AY, Suresh Kumar G, J. Biomol. Struct. Dyn 36 (2018) 2463–2473. [PubMed: 28760107]

[225]. Ladbury JE, Williams MA, Protein Rev, vol. 5, Springer, 2007, pp. 231–254.

[226]. Wang JC, Nat. Rev, Mol. Cell. Biol 3 (2002) 430–440. [PubMed: 12042765]

[227]. Tse-Dinh Y-C, Nucleic Acids Res. 37 (2009) 731–737. [PubMed: 19042977]

[228]. Vos SM, Tretter EM, Schmidt BH, Berger JM, Nat. Rev. Mol. Cell. Biol 12 (2011) 827–841. [PubMed: 22108601]

[229]. Nitiss JL, Nat. Rev, Cancer 9 (2009) 338–350. [PubMed: 19377506]

[230]. Pommier Y, ACS Chem, Biol. 8 (2013) 82–95. [PubMed: 23259582]

[231]. Kim KH, Lee MS, Nat. Rev. Endocrinol 10 (2014) 322–337. [PubMed: 24663220]

[232]. Rabinowitz JD, White E, Science 330 (2010) 1344–1348. [PubMed: 21127245]

[233]. Mizushima N, Komatsu M, Cell 147 (2011) 728–741. [PubMed: 22078875]

[234]. Das G, Shravage BV, Baehrecke EH, Cold Spring Harb. Perspect. Biol, vol. 4, 2012, pp. 10.1101/cshperspect.a008813a008813.

[235]. Heymann D, Curr. Opin, Investig. Drugs 7 (2006) 443–450.

[236]. Trejo-Solís C, Palencia G, Zuñiga S, Rodríguez-Ropon A, Osorio-Rico L, Torres Luvia S, Gracia-Mora I, Marquez-Rosado L, Sánchez A, Moreno-García ME, Cruz A, Bravo-Gómez ME, Ruiz-Ramírez L, Rodríquez-Enriquez S, Sotelo J, Neoplasia 7 (2005) 563–574. [PubMed: 16036107]

[237]. Galluzzi L, Larochette N, Zamzami N, Kroemer G, Oncogene, vol. 25, 2010, pp. 4812–4830.

[238]. Gogvadze V, Zhivotovsky B, Orrenius S, Mol. Asp. Med 31 (2010) 60–74.

[239]. Qi F, Li A, Inagaki Y, Xu H, Wang D, Cui X, Zhang L, Kokudo N, Du G, Tang W, Food Chem, Toxicol. 50 (2012) 295–302. [PubMed: 22019693]

[240]. Renault TT, Chipuk JE, Chem. Biol 21 (2014) 114–123. [PubMed: 24269152]

[241]. Wagenblast E, Soto M, Gutiérrez-Ángel S, Hartl CA, Gable AL, Maceli AR, Erard N, Williams AM, Kim SY, Dickopf S, Harrell JC, Smith AD, Perou CM, Wilkinson JE, Hannon GJ, Knott SRV, Nature 520 (2015) 358–362. [PubMed: 25855289]

[242]. Wang R, Jin C, Hu X, Oncotarget 8 (2017) 41113–41124. [PubMed: 28467802]

[243]. Matt S, T.G, Cell. Mol. Life Sci, Hofmann, 2016.

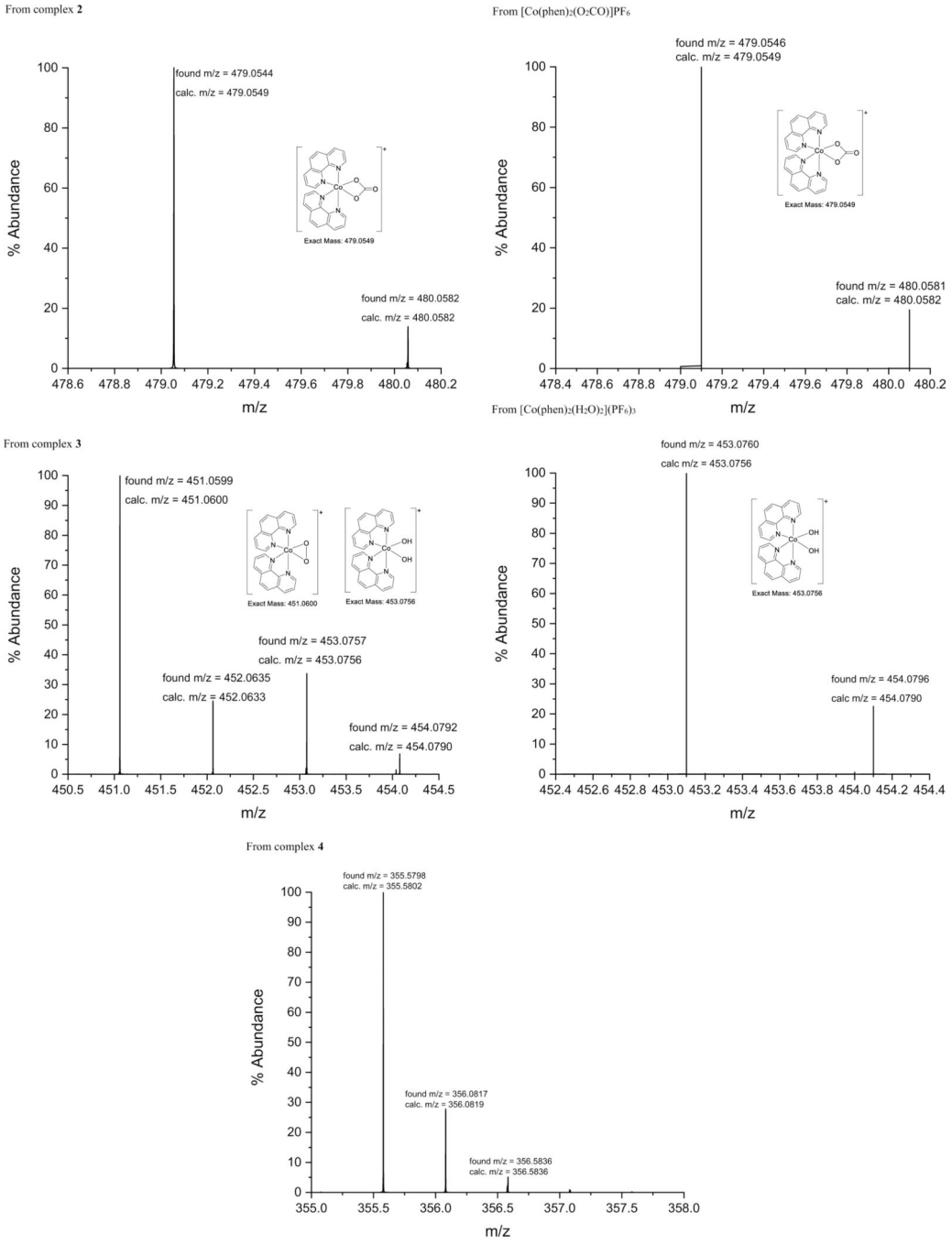

Fig. 1.

High resolution mass spectra (HRMS) of the cationic species formed from complex **2**, $[Co(phen)_2(O_2CO)]PF_6$, **3**, $[Co(phen)_2(H_2O)_2](PF_6)_3$, and complex **4** (in the positive mode).

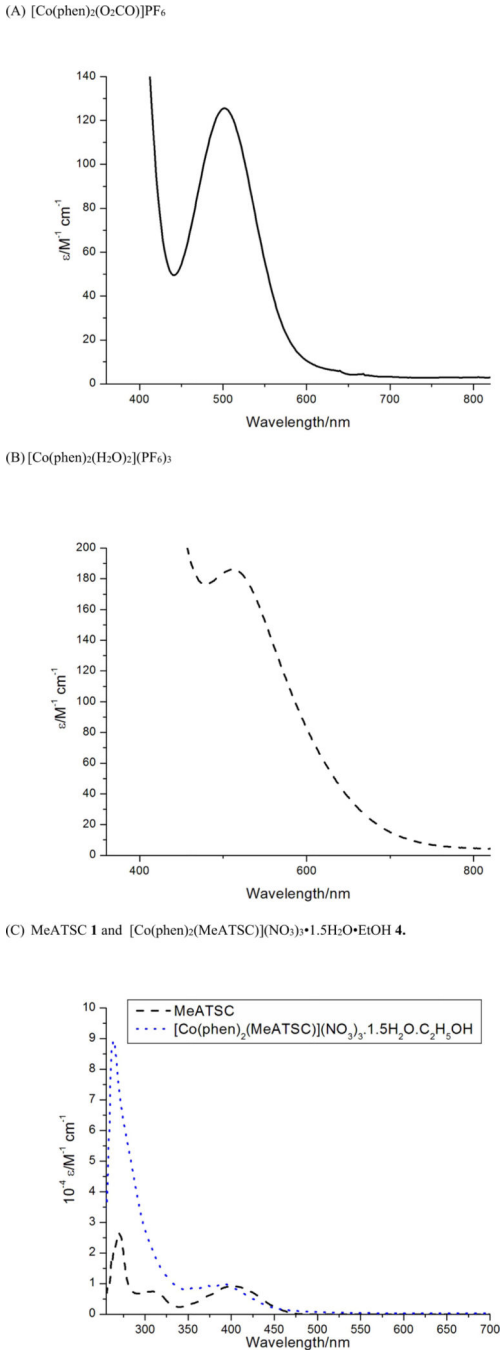

Fig. 2.

UV–visible spectra of MeATSC **1** and the respective cobalt(III) complexes in DMSO.

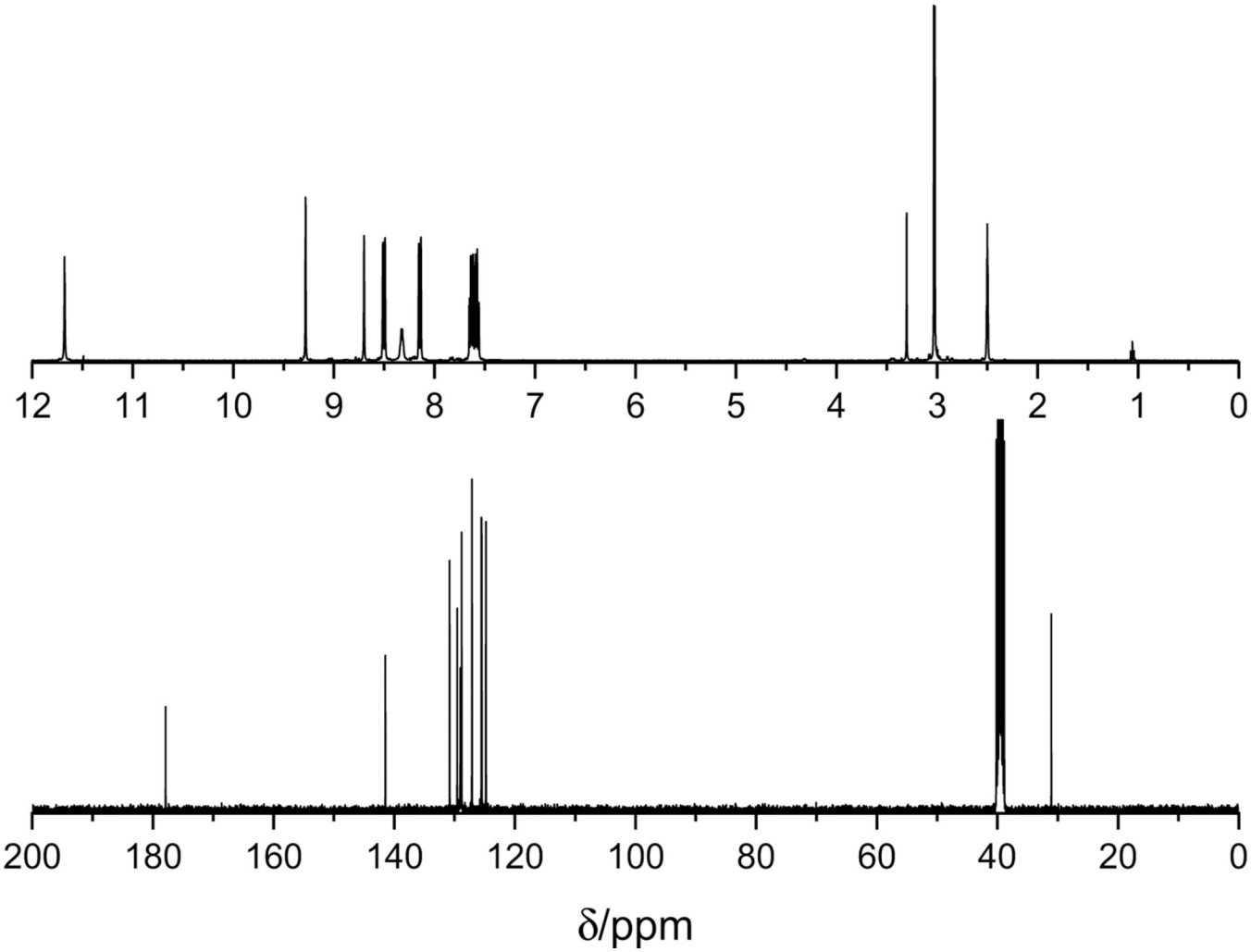

Fig. 3.
^{1}H and ^{13}C NMR spectra of MeATSC **1** in DMSO−d_6.

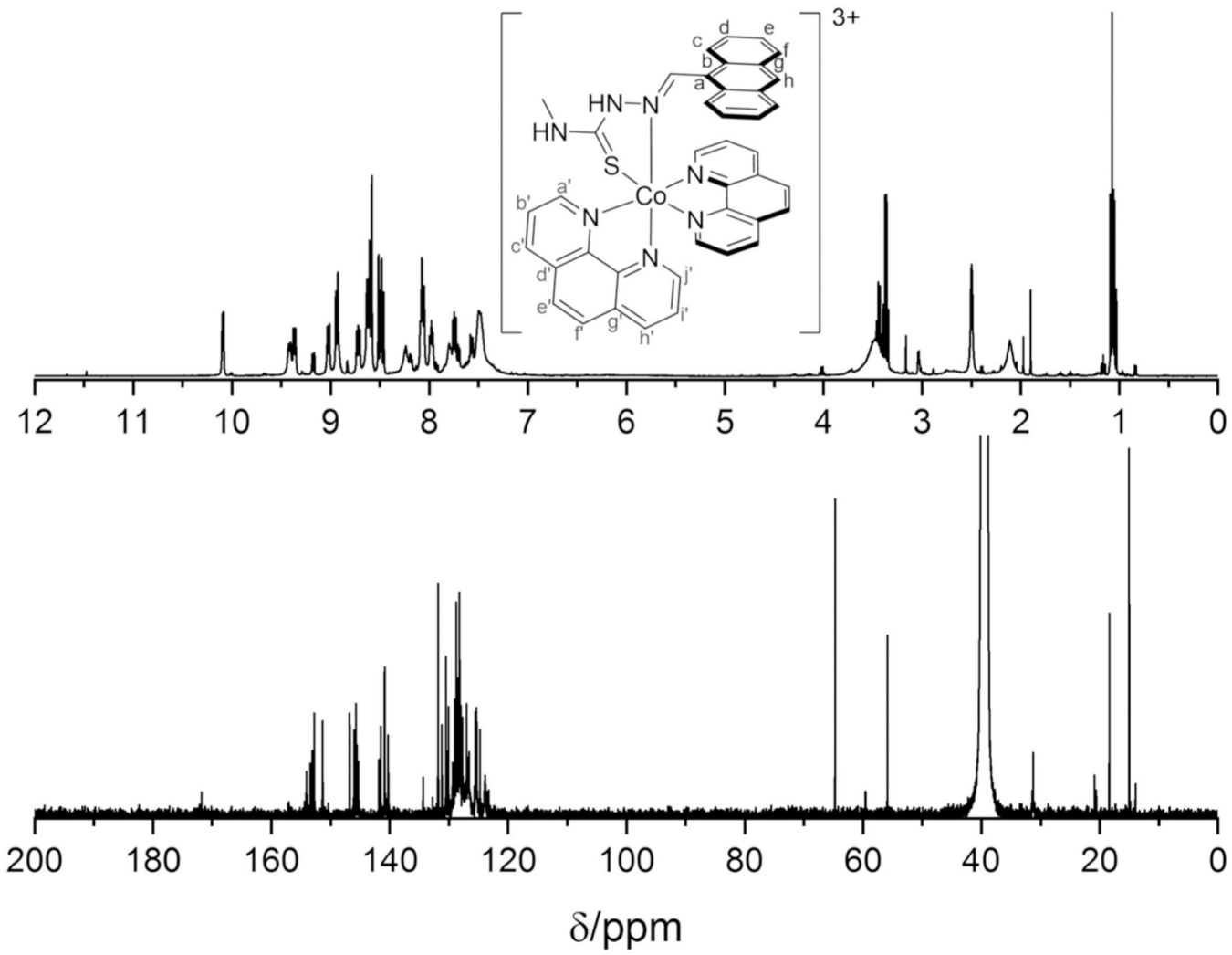

Fig. 4.

^{1}H and ^{13}C NMR spectra of complex **4** in DMSO−d_6.

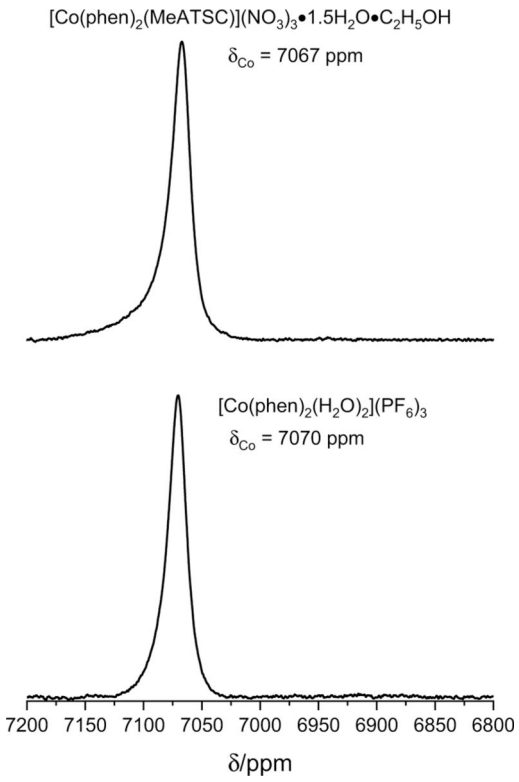

Fig. 5.

^{59}Co NMR spectra of $[Co(phen)_2(H_2O)_2](PF_6)_3$ and complex **4** in DMSO−d_6. [$[Co(phen)_2(H_2O)_2](PF_6)_3$] = 138 mM and [complex **4**] = 93 mM.

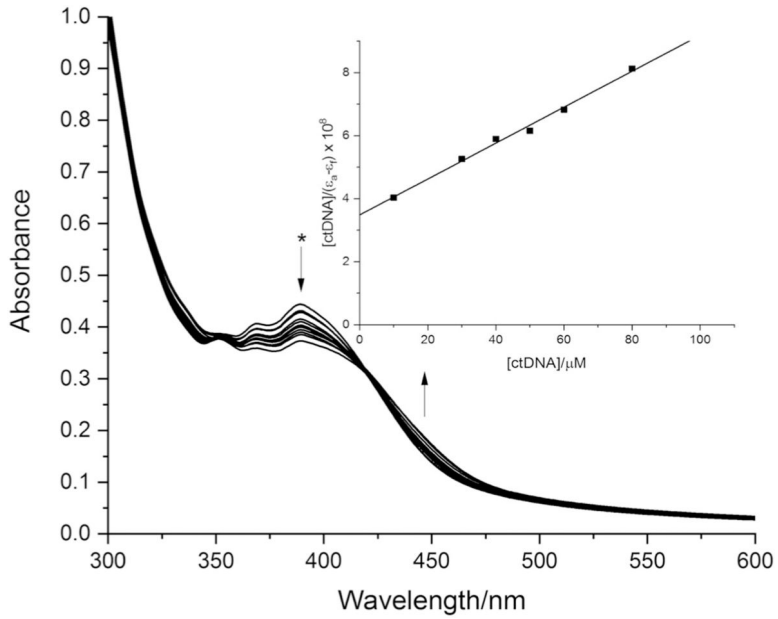

Fig. 6.

UV–visible spectra of the spectrophotometric titration of complex **4** with ctDNA. Inset: A plot of [ctDNA]/($\varepsilon_a - \varepsilon_f$) vs [ctDNA]. [complex] = 50 μM; pH = 7.72 ± 0.03; and Tris-HCl buffer ([Tris] = 5 mM, [HCl] = 3.55 mM, and [NaCl] = 25 mM). Arrow indicates the change upon increasing ctDNA concentration. Inset: A plot of [ctDNA]/($\varepsilon_a - \varepsilon_f$) vs [ctDNA].

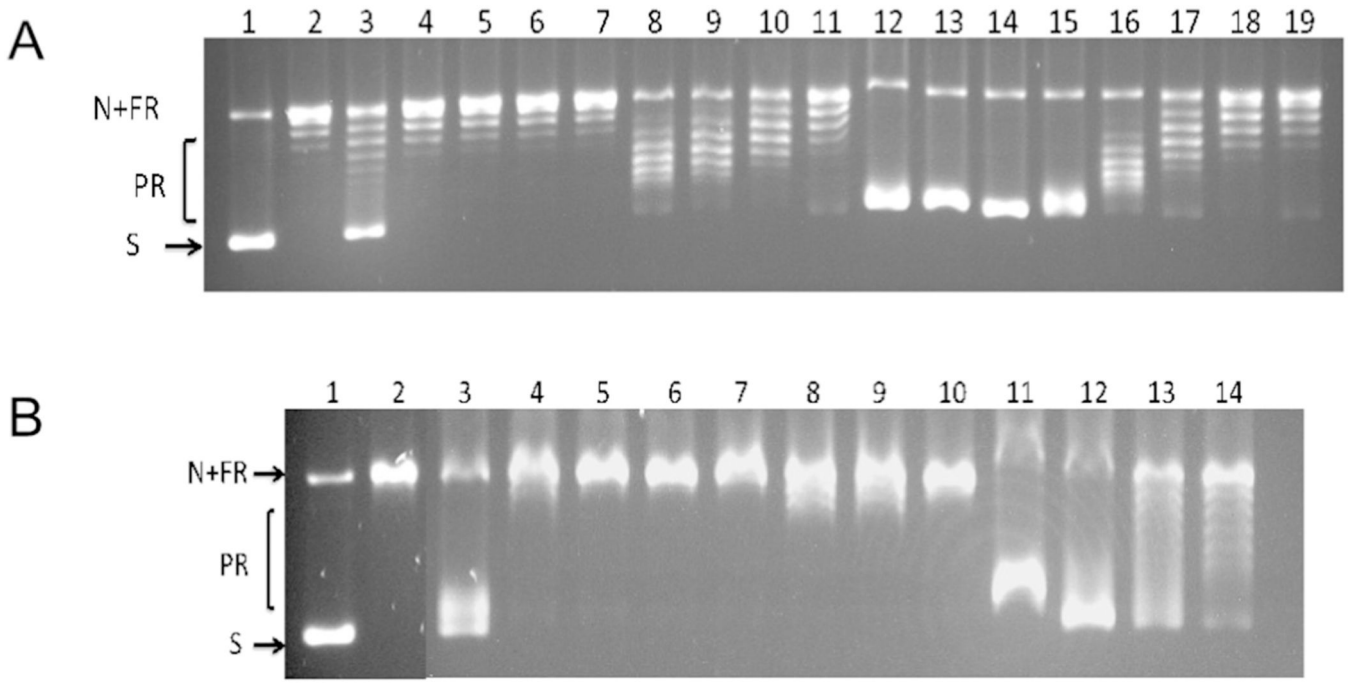

Fig. 7.

Agarose gels showing activity of hTOP1 relaxation activity in the presence of complex **4** and controls. A) Inhibition of hTOP1 relaxation activity by complex **4**. Lane 1: negatively supercoiled pBAD/Thio plasmid DNA; lane 2: DMSO as negative control; lane 3: positive control camptothecin at 100 μM; lanes 4–7: 100, 50, 25, and 12.5 μM $[Co(phen)_2(H_2O)_2](NO_3)_3$ **3**; lanes 8–11: 100, 50, 25, and 12.5 μM MeATSC **1** ligand; lanes 12–19: 101.8, 50.9, 25.5, 12.7, 6.4, 3.2, 1.6, and 0.8 μM complex **4**. B) Inhibition of hTOP2α relaxation activity by complex **4** (results are from the same agarose gel). Lane 1: negatively supercoiled pBAD/Thio plasmid DNA; lane 2: DMSO as negative control; lane 3: positive control *m*AMSA at 75 μM; lanes 4–7: 100, 50, 25, and 12.5 μM $[Co(phen)_2(H_2O)_2](NO_3)_3$ **3**; lanes 8–10: 100, 50, and 25 μM MeATSC ligand **1**; lanes 11–14: 101.8., 50.9, 25.5, and 12.7 μM complex **4**. N: nicked, FR: fully relaxed, PR: partially relaxed, S: supercoiled.

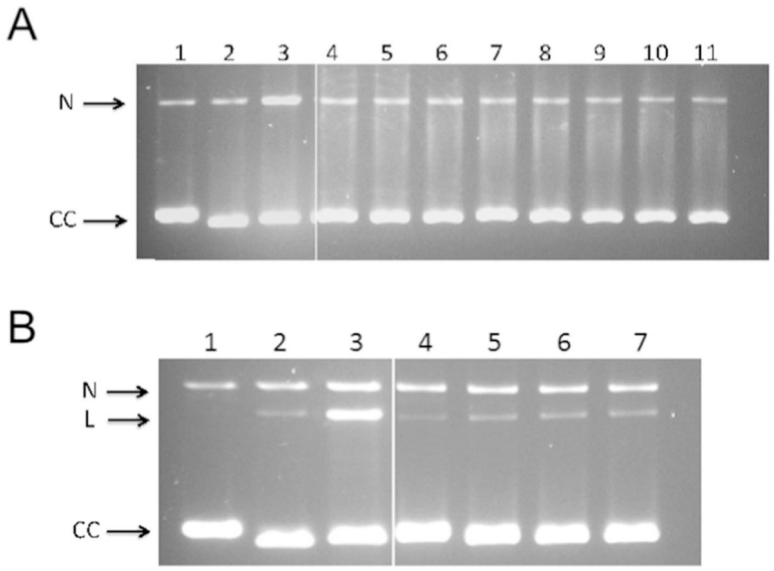

Fig. 8.

Agarose gels with DNA cleavage by hTOP2α in the presence of complex **4** and controls. (A) No increase in DNA cleavage product by hTOP1 in the presence of cobalt complex **4** (results are from the same agarose gel). Lane 1: negatively supercoiled pBAD/Thio plasmid DNA; lane 2: DMSO as negative control; lane 3: positive control camptothecin at 100 μM; lanes 4–11: 101.8, 50.9, 25.5, 12.7, 6.4, 3.2, 1.6, and 0.8 μM complex **4**. (B) Decrease in DNA cleavage product by hTOP2α in the presence of complex **4** (results are from the same agarose gel). Lane 1: negatively supercoiled pBAD/Thio plasmid DNA; lane 2: DMSO as negative control; lane 3: positive control *m*AMSA at 25 μM; lanes 4–7: 50.9, 25.5, 12.7, and 6.4 μM complex **4**. N: nicked, L: linear, CC: covalently closed. Gel electrophoresis was conducted in the presence of ethidium bromide so that relaxed DNA would migrate together with supercoiled DNA as covalently closed DNA, and separate from nicked DNA.

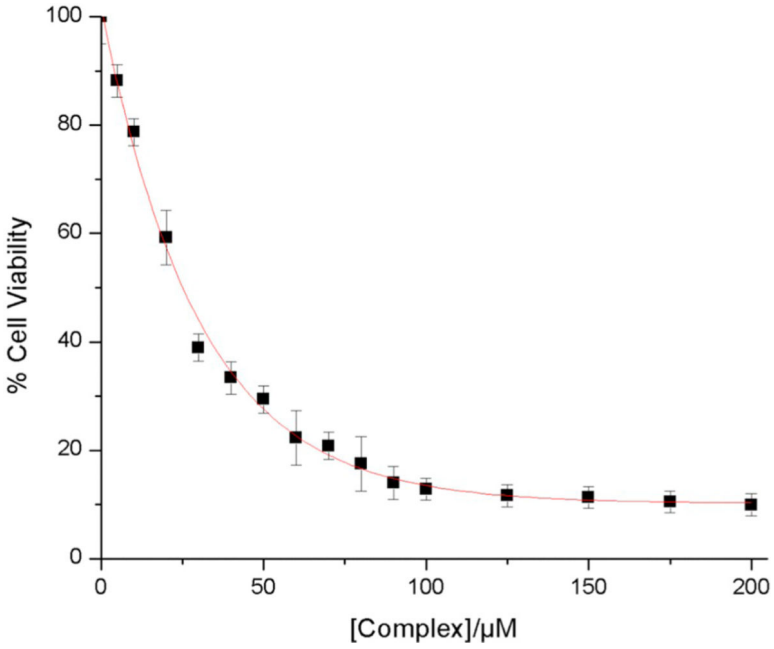

Fig. 9.

A plot of % cell viability versus concentration of complex **4**.

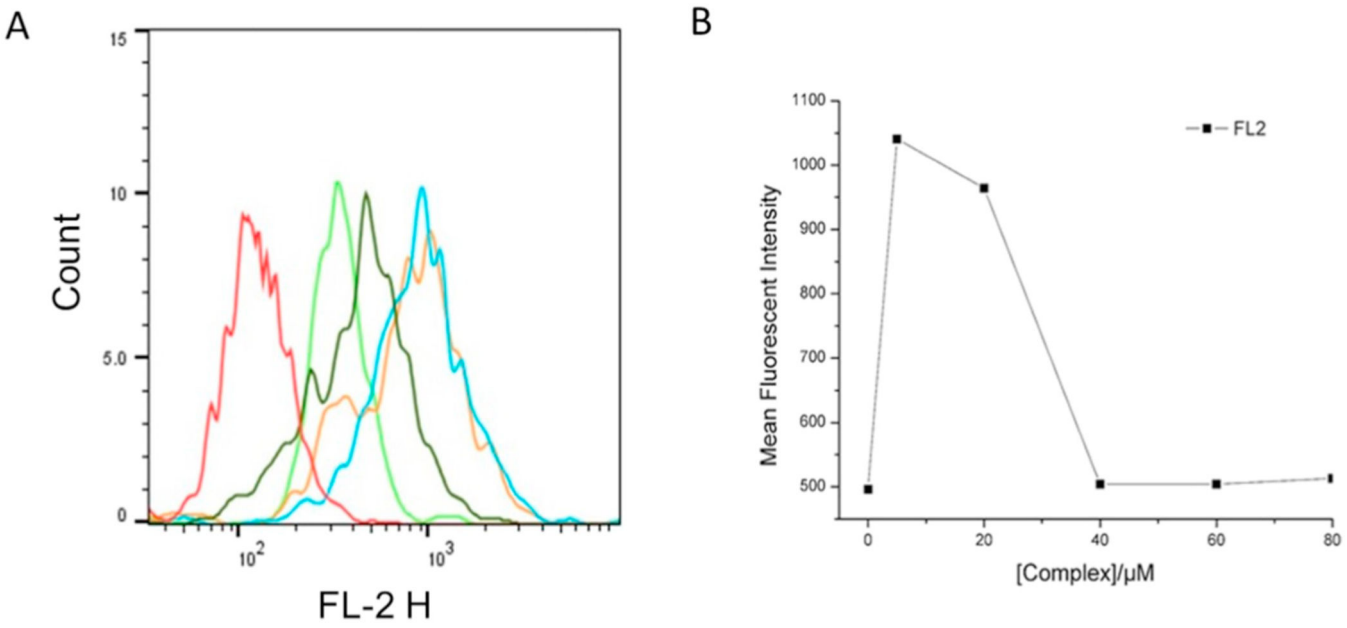

Fig. 10.

Effect of the concentration of complex **4** on autophagic flux in 4T1-luc cells. Complex **4** induces autophagic flux in 4T1-luc cells – (A) Representative histograms showing fluorescence resulting from autophagic flux (FL2-H, x-axis) and cell counts (y-axis) after incubation with complex **4** for 24 h. Red – unstained cells, dark green – 0 μM, cyan – 5 μM, yellow – 10 μM, and lime green – 80 μM. (B) Plot of the mean fluorescent intensity (515–545 nm) vs various concentrations of complex **4** after 24 h incubation. (For interpretation of the references to color in this figure legend, the reader is referred to the web version of this article.)

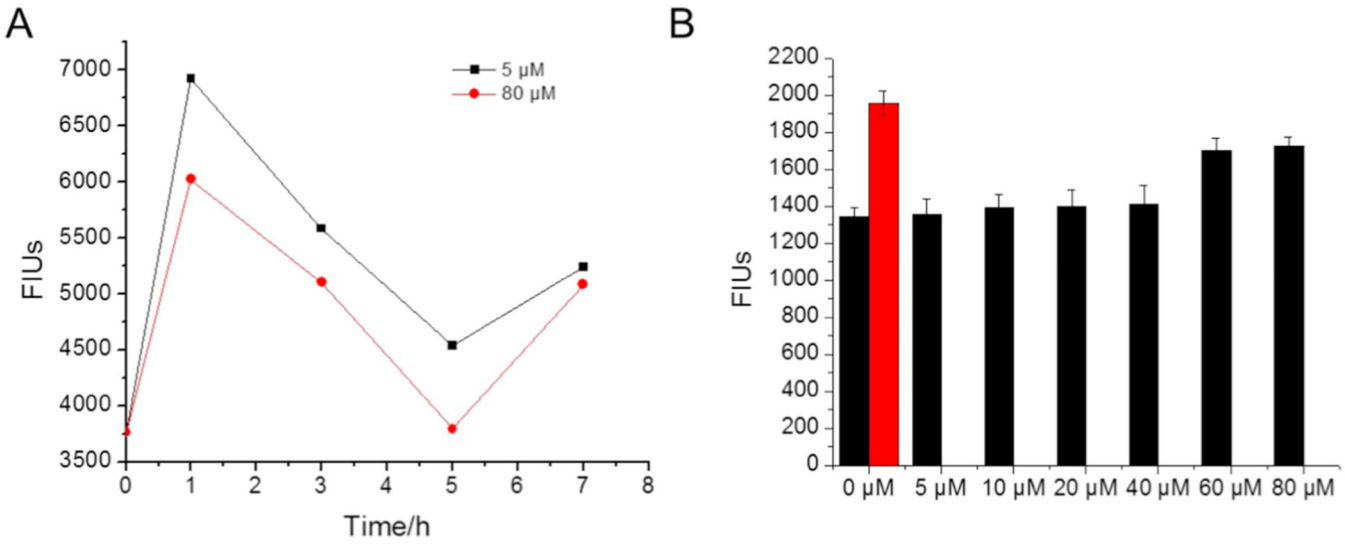

Fig. 11.

Effect of complex **4** on autophagic flux and its effect on autophagy in the presence of necrostatin-1 inhibition of autophagy. (A) Time-dependent effects of low and high concentrations of complex **4** on autophagic flux – 4T1-luc cells were treated with 5 μM (black) and 80 μM (red) complex **4** and autophagic flux was determine at the indicated times by fluorescence intensity on flow cytometry. (B) Effect of complex **4** on autophagy in the presence of necrostatin-1 inhibition of autophagy. Black color: drug treated cells and red: positive control (starvation). Data represents 20,000 molecular events collected4T1-luc cells were preincubated with 600 nM necrostatin-1 for 4 h. Cells were then washed and incubated with the indicated concentrations of complex **4** for 24 h and then analyzed for autophagy by flow cytometry. FUI: fluorescence units intensity at 515–545 nm. (For interpretation of the references to color in this figure legend, the reader is referred to the web version of this article.)

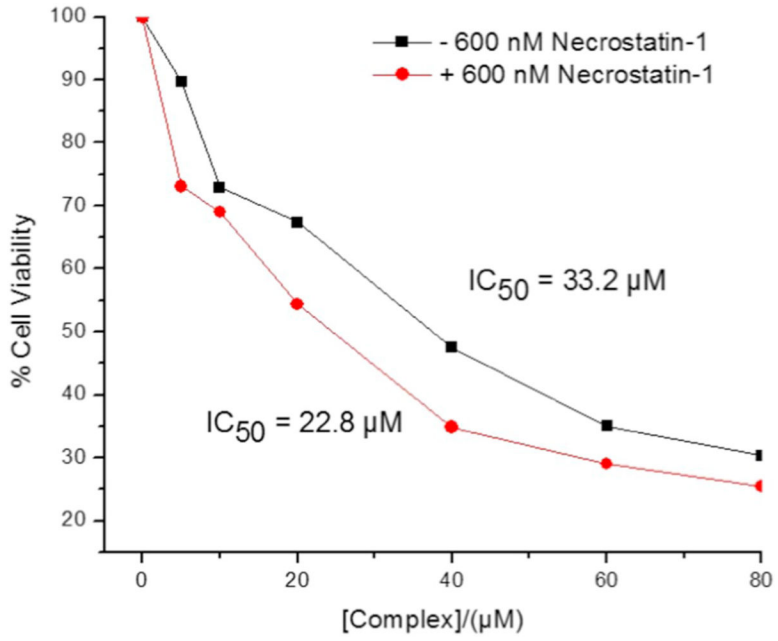

Fig. 12.

Cell viability following treatment of 4T1-luc cells with complex **4** in the presence or absence of necrostatin-1. Cells were seeded at 2.5×10^4 cells per well for 24 h prior to addition to treatment. Graphs represent n = 3 replicates of data with plates being 1 h post incubation with MTS reagent. Data was fit using an exponential function using Origin 8 software.

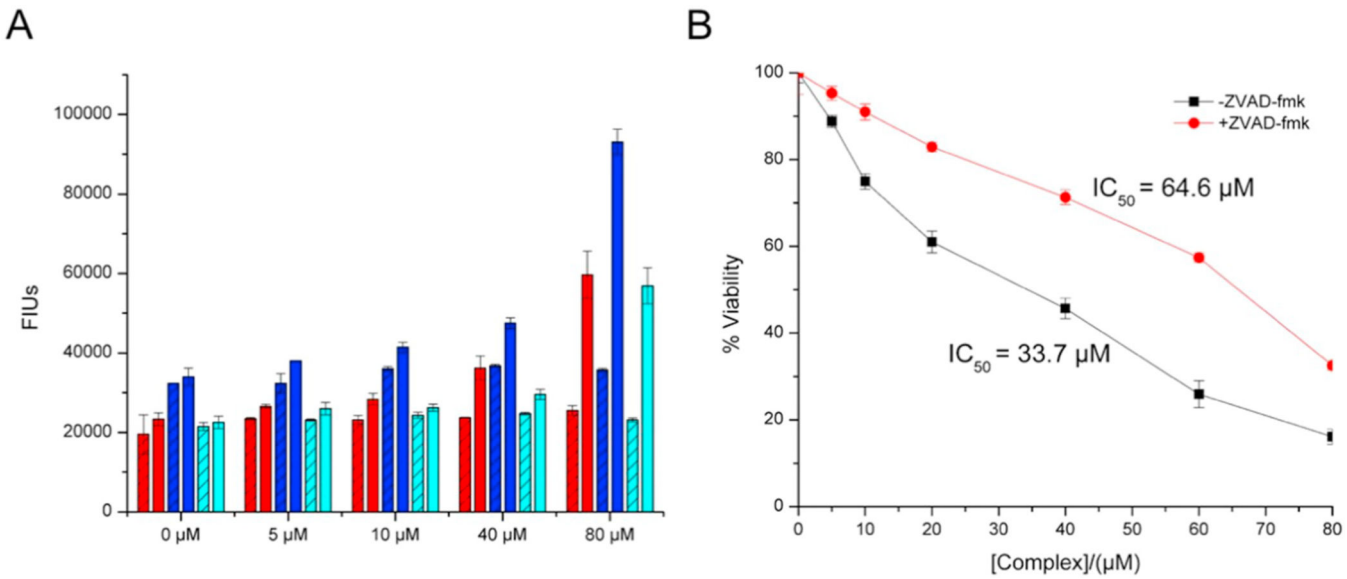

Fig. 13.

The effect of the concentration of complex **4** on caspase 3/7 catalytic activity in the absence and presence of pan caspase inhibitor z-VAD-FMK. A) Complex **4** induces increases in caspase 3/7 catalytic activity in 4T1-luc cells in a concentration- and time-dependent manner. 4T1-luc cells were preincubated in the presence (stripped bars) or absence (open bars) of 10 μM pan caspase inhibitor z-VAD-FMK for 4 h followed by exposure to complex **4** for various time: 1 h (red), 3 h (blue), 5 h (cyan). The activity of caspase-3/7 was measured using Caspase-Glo assay with DEVD-aminoluciferin as a substrate. (B) Cellular viability following exposure to complex **4** drastically increased when caspase 3 activity inhibited via z-VAD-FMK. 4T1-luc cells were pre-incubated for 4 h in the absence (black) or presence (red) of z-VAD-FMK and then treated with complex **4** at the indicated concentrations. Values from each point were normalized to control values. Values represent the mean ± SE (n = 3). (For interpretation of the references to color in this figure legend, the reader is referred to the web version of this article.)

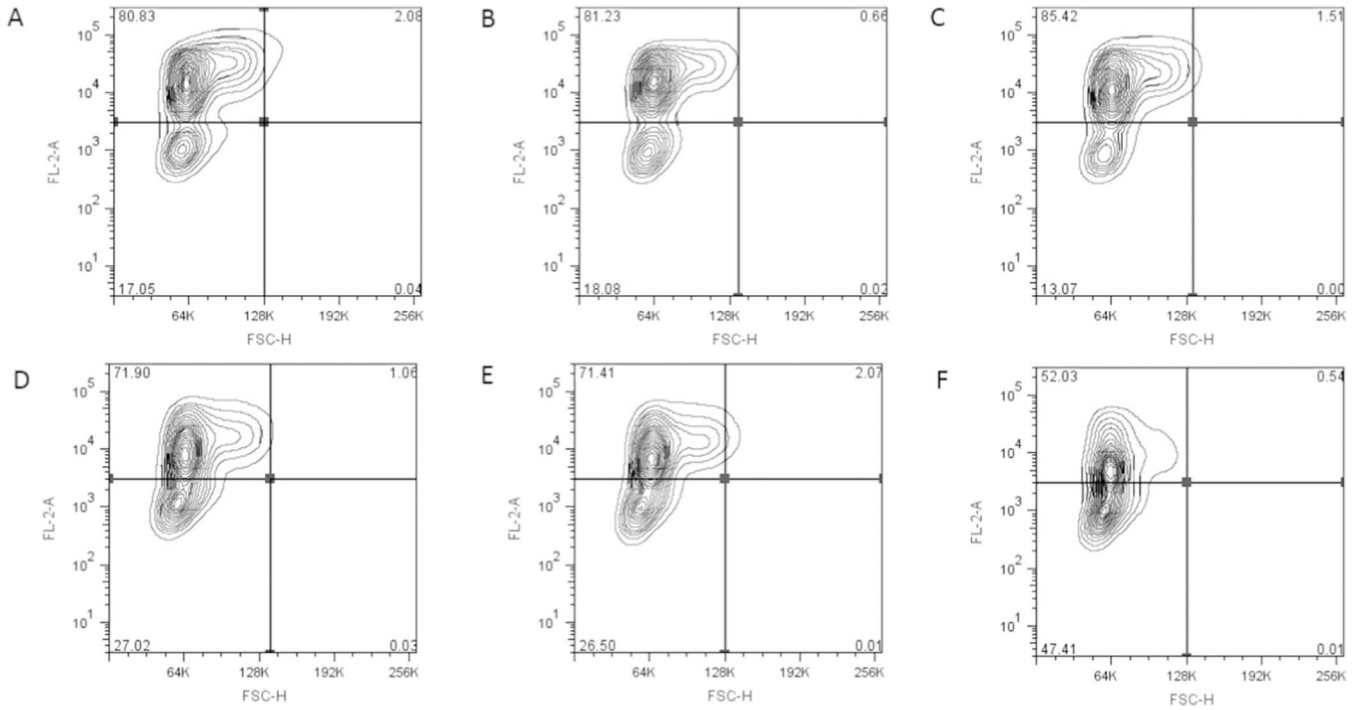

Fig. 14.

Effect of the concentration of complex **4** on the mitochondria membrane potential. Complex **4** causes mitochondria membrane potential ($\Delta\Psi_m$) dissipation in 4T1-luc cells – The $\Delta\Psi_m$ was determined in 4T1 cells 2 h after incubation with various concentration of complex **4**: (A) 0 μM, (B) 5 μM, (C) 20 μM, (D) 40 μM, (E) 60 μM, and (F) 80 μM. Representative contour plots are shown with TMRE fluorescence resulting from $\Delta\Psi_m$, (FL2-A, y-axis) and FSC-H (x-axis).

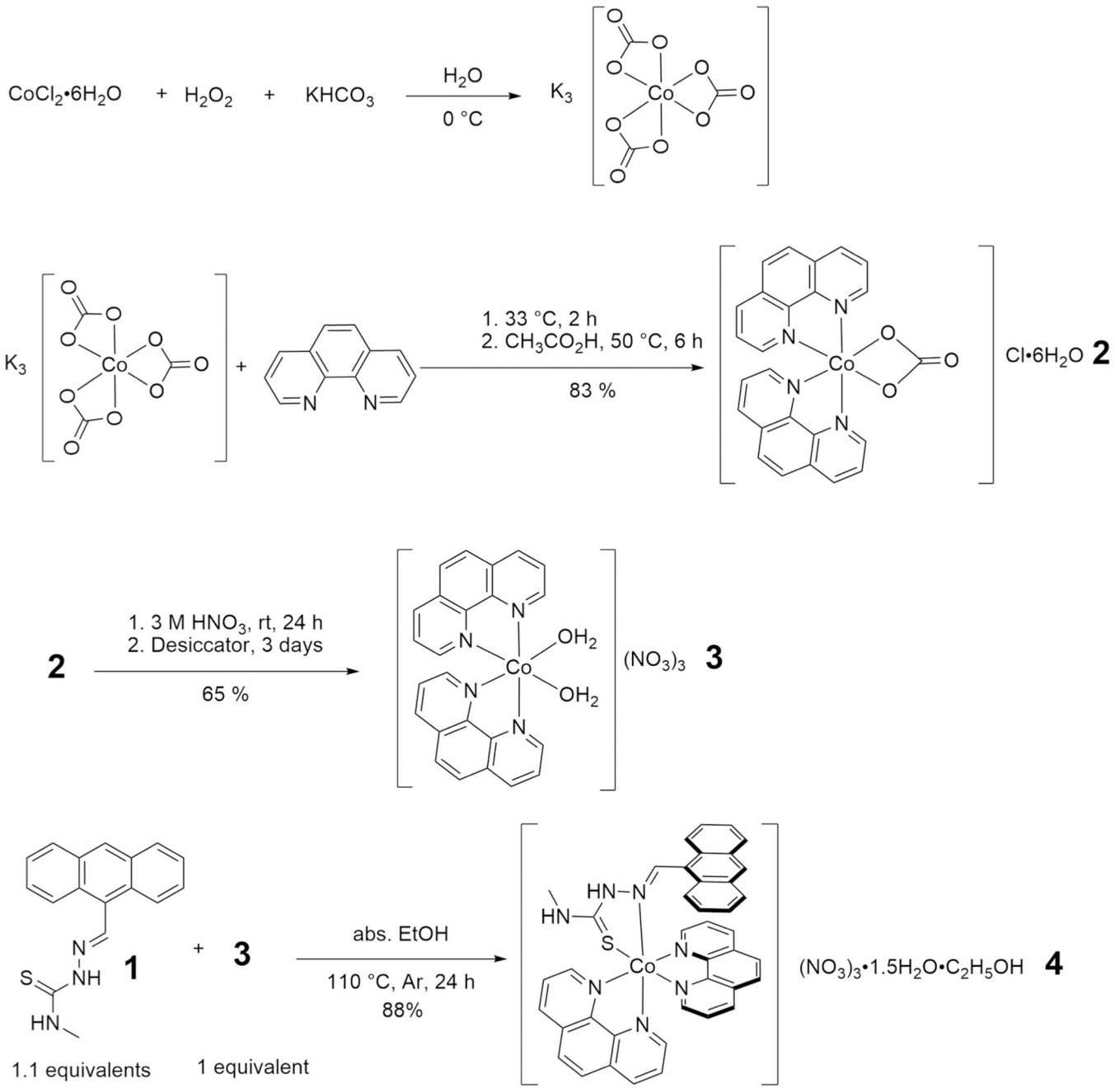

Scheme 1.

Synthesis of $[Co(phen)_2(MeATSC)](NO_3)_3 \cdot 1.5H_2O \cdot C_2H_5OH$ **4**.

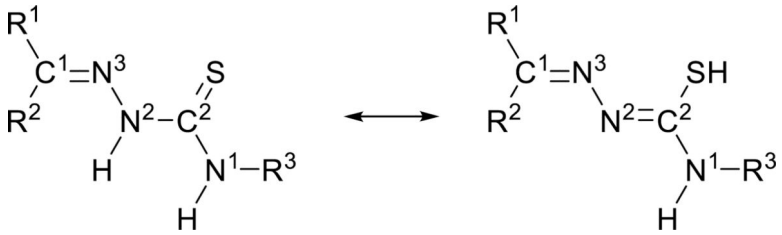

Scheme 2.
Tautomerism in thiosemicarbazones [140].

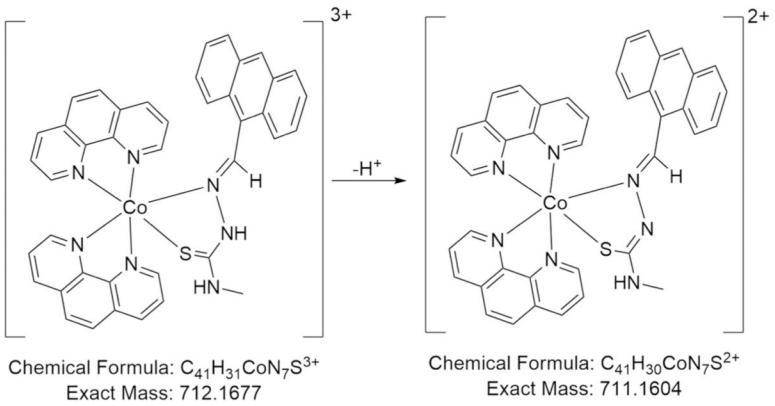

Scheme 3.

Tautomerism of a thiosemicarbazone and the proposed mechanism for the formation of the doubly charged cation from complex **4** in the mass spectrometer.

Table 1

FT IR spectroscopic data for the ligand and complexes. Units = cm^{-1}.

Species	$-N^1H_2$ ν(NH)	N^2H ν(NH)	ν(N–N)	ν(C═N)	ν(C═S)	ν(NO_3^-)
MeATSC **1**	3397 (m)	3200 (m)	1075 (s)	1620 (m)	1254 (s), 841 (s)	–
Complex **4**	3227 (s, br)	3053 (s, br)	–	1580 (m)	1224 (s), 827 (s)	1323 (vs)
[VO(sal-*L*-tryp)(MeATSC)]·1.5C_2H_5OH[a]	3340 (m)	2976 (w)	1148 (m)	1620 (m)	1225 (m), 829 (m)	–

[a]Ref. [161].

Table 2

UV-visible spectroscopic data for the respective species in DMSO.

Species	λ/nm	10^{-4} ε/ M^{-1} cm^{-1}	λ/nm	10^{-4} ε/ M^{-1} cm^{-1}	λ/nm	10^{-4} ε/ M^{-1} cm^{-1}	λ/nm	10^{-4} ε/M^{-1} cm^{-1}
1	269	2.6	309	0.74	403	0.91	—	—
2	—	—	—	—	—	—	502	0.0126
3	—	—	—	—	—	—	513	0.0186
4	264	8.9	355	0.85	372	0.93	392	1.0

1 = MeATSC, **2** = complex **2** as a PF_6^- salt, $[Co(phen)_2(O_2CO)]PF_6$, **3** = complex **3** as a PF_6^- salt, $[Co(phen)_2(H_2O)_2](PF_6)_3$, and **4** = $[Co(phen)_2(MeATSC)](NO_3)_3 \cdot 1.5H_2O \cdot C_2H_5OH$.

Table 3

A dose-response and time course for complex 4 effects on the 4T1-luc cell's mitochondria membrane potential. Percentages of cells with a high $\Delta\Psi_m$, (positive) and low $\Delta\Psi_m$, (negative) for TMRE fluorescence after 2, 4, and 6 h.

[Complex 4]/μM	2 h		4 h		6 h	
	–	+	–	+	–	+
0	17.05	80.83	24.92	73.21	16.96	78.88
5	18.08	81.23	36.63	60.72	14.16	79.37
20	13.07	85.42	48.76	49.73	31.86	61.65
40	27.02	71.9	42.35	55.63	50.11	46.01
60	26.5	71.41	39.93	58.44	52.42	45.26
80	47.41	52.03	17.33	80.58	45.21	53.42